

**ANNUAL TECHNICAL PROGRESS REPORT
OF THE RADIOISOTOPE POWER SYSTEMS
MATERIALS PRODUCTION AND
TECHNOLOGY PROGRAM TASKS
FOR OCTOBER 1, 2009 THROUGH
SEPTEMBER 30, 2010**

March 2011

**Prepared by
J. F. King**

DOCUMENT AVAILABILITY

Reports produced after January 1, 1996, are generally available free via the U.S. Department of Energy (DOE) Information Bridge.

Web site <http://www.osti.gov/bridge>

Reports produced before January 1, 1996, may be purchased by members of the public from the following source.

National Technical Information Service
5285 Port Royal Road
Springfield, VA 22161
Telephone 703-605-6000 (1-800-553-6847)
TDD 703-487-4639
Fax 703-605-6900
E-mail info@ntis.gov
Web site <http://www.ntis.gov/support/ordernowabout.htm>

Reports are available to DOE employees, DOE contractors, Energy Technology Data Exchange (ETDE) representatives, and International Nuclear Information System (INIS) representatives from the following source.

Office of Scientific and Technical Information
P.O. Box 62
Oak Ridge, TN 37831
Telephone 865-576-8401
Fax 865-576-5728
E-mail reports@osti.gov
Web site <http://www.osti.gov/contact.html>

This report was prepared as an account of work sponsored by an agency of the United States Government. Neither the United States Government nor any agency thereof, nor any of their employees, makes any warranty, express or implied, or assumes any legal liability or responsibility for the accuracy, completeness, or usefulness of any information, apparatus, product, or process disclosed, or represents that its use would not infringe privately owned rights. Reference herein to any specific commercial product, process, or service by trade name, trademark, manufacturer, or otherwise, does not necessarily constitute or imply its endorsement, recommendation, or favoring by the United States Government or any agency thereof. The views and opinions of authors expressed herein do not necessarily state or reflect those of the United States Government or any agency thereof.

Radioisotope Power Systems Materials Production and Technology Program
Materials Science and Technology Division

**ANNUAL TECHNICAL PROGRESS REPORT OF RADIOISOTOPE POWER
SYSTEMS MATERIALS PRODUCTION AND TECHNOLOGY PROGRAM
TASKS FOR OCTOBER 1, 2009 THROUGH SEPTEMBER 30, 2010**

J. F. King

March 2011

Prepared for
Department of Energy Office of Space and Defense Power Systems

Prepared by
OAK RIDGE NATIONAL LABORATORY
Oak Ridge, Tennessee 37831-6079
managed by
UT-BATTELLE, LLC
for the
U.S. DEPARTMENT OF ENERGY
under contract DE-AC05-00OR22725

CONTENTS

	Page
1. INTRODUCTION	1
2. PRODUCTION TASKS	2
2.1 CARBON-BONDED CARBON FIBER	2
2.1.1 Background	2
2.1.2 CBCF Process Development	2
2.1.3 CBCF Production	3
2.1.4 CBCF Qualification	3
2.1.5 CBCF Production and Qualification Procedures	4
2.1.6 CBCF Production and Qualification Capability	4
2.2 IRIDIUM ALLOY BLANK AND FOIL PRODUCTION	4
2.2.1 Blank Production	4
2.2.2 Powder Processing	5
2.2.3 Equipment Major Maintenance and Purchase	5
2.2.4 Training	6
2.2.5 Materials Characterization	6
2.2.5.1 Weldability Testing	6
2.2.5.2 Impurity Effects	6
2.2.6 Deviation Requests	6
2.2.7 Publications	7
2.3 CLAD VENT SET	9
2.3.1 Maintenance Production Summary	9
2.3.2 Nonconformance Reports	9
2.3.3 Deviation Requests	12
2.3.4 Evaluation of Aluminum on Iridium	12
2.3.5 Characterization of Scribed (Engraved) Identity Marks on CVS Cups	14
2.3.6 Decontamination Cover Tooling	20
2.3.7 Cup Sizing and Forming Evaluation Summaries	22
2.3.8 Frit Vent Tooling Evaluation	22
2.3.9 Metallurgical Destructive Test Sample Evaluations of Recrystallized and Sized Iridium Alloy Clad Vent Set Cup Conditions	24
2.3.10 Miscellaneous Maintenance Production	25
2.4 IRIDIUM POWDER AND INVENTORY MANAGEMENT	26
2.4.1 Iridium Demand and Supply Schedule	26
2.4.2 Annual Write-Off	27
2.4.3 Iridium Accountability Reviews	27

2.5	WELDING	28
2.5.1	Laser System	28
2.5.2	Electron Beam Welder	31
2.5.3	Flow Testing	33
3.	BASE TECHNOLOGY TASKS	34
3.1	ALLOY CHARACTERIZATION	34
3.2	ORNL Characterization of Min-K TE-1400 FY 2009	38
3.2.1	Introduction	38
3.2.2	Testing and Results of Changing Environments Testing	39
3.2.2.1	Experimental Procedures	39
3.2.2.2	Results	40
3.2.3	Testing and Results of Lateral Load Testing	46
3.2.3.1	Experimental Procedures	46
3.2.3.2	Results	46
3.2.4	Testing and Results of Isothermal Stress Relaxation Testing	55
3.2.4.1	Experimental Procedures	55
3.2.4.2	Results	56

LIST OF FIGURES

Figure	Page
1	Replacement water-cooling system for electron beam melting furnace was installed and made operational 8
2	Upgraded vacuum and emission control system for electron beam melting furnace was installed and became operational..... 8
3	“Black spot” area in the closure weld zone of shield cup assembly 974-05-5383. 3a) secondary electron image, 3b) backscattered electron image, 3c) elemental spectra, 3d-h) x-ray maps of aluminum, carbon, iridium, oxygen, and tungsten..... 10
4	Stylus 1 with diamond tip having 28° base angle, 124° tip entry angle, 765 µm maximum diameter, and 201 µm height 14
5	Backscattered electron image showing a typical “O” scribe mark (92 µm wide x 11.4 µm deep x 14.1° scribed base or wall angle) using a 1523 g load with surface cracking (tearing) – stylus # 6 on recrystallized Cup TC187 16
6	Backscattered electron image showing a typical “T” scribe mark (56 µm wide x 5.6 µm deep x 11.5° scribed base or wall angle) using a 435 g load with surface cracking (tearing) – stylus # 6 on recrystallized cup TC187..... 17
7	Backscattered electron image showing a typical “8” scribe mark (90 µm wide x 6.5 µm deep x 8.2° scribed base or wall angle) using a 1523 g load with no surface cracking – stylus # 9 on stress relieved blank RS12-5-4 (formed to make cup TC187) 18
8	Metallographically prepared Sample TC187-1 showing cross-section of “T” scribe mark made on recrystallized material using a 435 g load. The depth of strain below the mark is ~14 µm 19
9	Metallographically prepared Sample TC187-3 showing cross-section of “O” scribe mark made on recrystallized material using a 1523 g load. The depth of strain below the mark is ~42 µm 20
10	Alternate designs for ATJ graphite sintering Pins to avoid contact with iridium frit vent powder during the vacuum sintering operation..... 23

Figure	Page
11 ATJ graphite Cover to be placed over a sintering fixture so that Pins would not be required, yet the iridium frit vent powder would be shielded during the vacuum sintering operation	24
12 Updated Production Laser Welding System.....	29
13 New Electronics Upgrade	30
14 Modified Rotary Positioner.....	31
15 Weld Cross Section Between Two Stainless Steel Waster Sheets Used to Encapsulate an Iridium Blank for Forming	32
16 Remanufactured Ten Head Weld Positioner Installed on the Slide Table.....	33
17 Temperature dependence of the tensile stress-strain curves of DOP-26 iridium at an engineering strain rate of $\sim 10 \text{ s}^{-1}$. The grain size was $\sim 40 \mu\text{m}$	35
18 Temperature dependence of the tensile stress-strain curves of DOP-26 iridium at an engineering strain rate of $\sim 1 \text{ s}^{-1}$. The grain size was $\sim 40 \mu\text{m}$	36
19 Comparison of the mechanical properties of DOP-26 iridium at two different strain rates of 10 s^{-1} and 1 s^{-1}	37
20 Results from Changing Environments Test #1_3	41
21 Results from Changing Environments Test #1_3	41
22 Changing Environment Event One for Test #1_6.....	42
23 Changing Environment Event Two for Test #1_6.....	42
24 Changing Environment Event Two for Test #1_6.....	43
25 TSE Test for Test #1_6.....	43
26 Results from Changing Environments Test #1_7	44
27 Changing Environment Event One for Test #1_7.....	45
28 Changing Environment Event Two for Test #1_7.....	45
29 TSE Test for Test #1_7.....	46

Figure	Page
30 Results for 1" Samples Using Lateral Load Testing Set-Up after First Modification.....	51
31 Results for 2.5" Square Sample Using Lateral Load Testing Set-Up after First Modification Using Step Unloading	52
32 Results for Lateral Step Loading of 1" Square Sample Using Lateral Load Testing\Set-Up after Second Modification	53
33 Characteristic Results for Lateral Step Loading of 1" Square Sample Loaded to 65 lbs. Axially.....	53
34 Isothermal Test #3_11 (650°C).....	56

LIST OF TABLES

Table		Page
1	Scribe Data Summary for “0” Scribed with Nine Styli Using 1523 g Load on Recrystallized Cup TC187	15
2	Scribe Data Summary for “T” Scribed with Nine Styli Using 435 g Load on Recrystallized Cup TC187	15
3	Scribe Data Summary for Three Figures Made Using 1523 g Load on Stress Relieved Blank RS12-5-4 (Later Formed to Make Cup TC187).....	17
4	Microhardness Results for Cups in Three Conditions: As-Recrystallized, Sized/Recrystallized, and Recrystallized/Sized.....	24
5	Demand and Supply Schedule Shows Factors and Provides Strategy to Ensure an Adequate Supply of Iridium Powder for NASA Space Explorations and Defense Missions.....	27
6	Changing Environments Test Matrix.....	39
7	Initial Lateral Load Testing Results	47
8	Lateral Load Test Matrix Utilizing Modified Test Frame	48
9	Summary of General Lateral Load Test Results After Second Modification.....	55
10	Isothermal Stress Relaxation Test Matrix.....	56

ACRONYMS

AA	aluminum alloy
CBCF	Carbon-Bonded Carbon Fiber
CNC	Computer Numerical Control
CVS	Clad Vent Set
DAQ	data acquisition
DOE	Department of Energy
DR	deviation request
EBM	electron beam melting
EDM	electro discharge machined
EBW	electron beam welder
FVA	frit vent assembly
FY	fiscal year
INL	Idaho National Laboratory
LANL	Los Alamos National Laboratory
NASA	National Aeronautics and Space Administration
ORNL	Oak Ridge National Laboratory
NCR	nonconformance reports
QA	quality assurance
RPS	Radioisotope Power Systems
RTG	radioisotope thermoelectric generators
SEM	scanning electron microscope
VCA	vent cup assemblies
VMM	vision measuring machine

**ANNUAL TECHNICAL PROGRESS REPORT OF RADIOISOTOPE POWER
SYSTEMS MATERIALS PRODUCTION AND TECHNOLOGY PROGRAM
TASKS FOR OCTOBER 1, 2008 THROUGH SEPTEMBER 30, 2009***

J. F. King

1.0 INTRODUCTION

The Office of Radioisotope Power Systems of the Department of Energy (DOE) provides Radioisotope Power Systems (RPS) for applications where conventional power systems are not feasible. For example, radioisotope thermoelectric generators were supplied by the DOE to the National Aeronautics and Space Administration (NASA) for deep space missions including the Cassini Mission, Pluto New Horizons, and the Mars Science Laboratory. ORNL produced carbon-bonded carbon fiber (CBCF) insulator sets, iridium alloy blanks and foil, and clad vent sets (CVS) used in these generators. The Oak Ridge National Laboratory (ORNL) has been involved in developing materials and technology and producing components for the DOE for nearly four decades.

This report reflects program guidance from the Office of RPS for fiscal year (FY) 2010. Production activities for prime quality (prime) CBCF insulator sets, iridium alloy blanks and foil, and CVS are summarized in this report. Technology activities are also reported that were conducted to improve the manufacturing processes, characterize materials, or to develop information for new RPS.

*Research sponsored by the U.S. Department of Energy, Office of Space and Defense Power Systems, under contract with UT-Battelle, LLC.

2.0 PRODUCTION TASKS

2.1 CARBON-BONDED CARBON FIBER

2.1.1 Background

The CBCF production facilities have been operated in a production maintenance mode since the Cassini campaign to produce prime quality insulators. Dedicated facilities for CBCF production remain in the Carbon Materials Technology Laboratory at ORNL. During much of the 1990s CBCF production was directed at making experimental variations of CBCF that explored the potential for improved insulating attributes at very high temperatures. The effect of brief excursions to reentry temperatures was also explored. Sleeves produced in FY 2000 were the first to be fully characterized in nearly a decade. Resolution of issues related to elevated impurities in CBCF allowed for continued production of prime quality insulators in FY 2003 through FY 2010. Prime quality insulation sets were shipped to Idaho National Laboratory (INL) in FY 2006 through FY 2008 to support the Mars Science Laboratory Mission. Production of prime quality insulators continued in FY 2010 while implementing upgrades to production equipment and revision of numerous procedures.

2.1.2 CBCF Process Development

The vacuum molding system was refitted with a new flow meter, flow control valve and electronic controller. The flow meter and flow control valve are identical to the original units. The new electronic controller is similar to the original in function but different in make, model and details of operation. Integrated operation of the controller and valve required a multitude of trial molding runs to establish appropriate control parameters (gain, reset rates, filter levels, etc.) that resulted in stable response of the valve. The system was tuned such that instantaneous slurry flow rates matched the programmed set point values within $\pm 2\%$.

Once system control was established, numerous molding runs were made of CBCF sleeve billets and plates to define a flow rate program that would ultimately result in carbonized billets and plates of desired density and strength. Other requirements of the specification are generally less problematic. In the case of CBCF sleeve billets, the initial slurry flow rate during vacuum molding must be sufficient to retain fiber and resin at the vertical mold surface and continue to support the growing thickness of the composite. The flow rate is typically increased by a factor of two from the beginning to the end of molding. Total molding times were nominally within the historic values. Higher slurry flow rates during vacuum molding generally result in greater compaction of the fibers and, consequently, higher final density. Determination of the density (or strength) of CBCF billets and plates requires: carbonization of rayon, slurry preparation, vacuum molding, drying, curing, carbonization, machining of specimens, 40 hour outgassing of specimens and finally property measurement. Density was often measured after carbonization on a machined sleeve or disc blank. Sleeve billets within the upper range of the density specification were produced.

In the case of CBCF plates for discs, eight plates were produced with a variety of flow rates. The final density for these plates was at or above the upper limit of the density specification. During these test runs and FY 2010 production runs it became apparent that significant compaction of the wet CBCF preform occurred at the very onset of vacuum dewatering, before air began to flow through the composite. During this brief period, the surface of the fragile composite is subjected to full atmospheric pressure (14.7 psi). This phenomenon is also operative during vacuum molding of sleeve billets. Before the beginning of process development in FY 2010, a new mold was made for plate production since an extensive crack had developed in the weld of the original mold. The seal with the vacuum manifold base was also improved to minimize excessive clearance. It later became obvious that these leaks had served as a vacuum relief valve during dewatering of plate billets in past production. Closing the leaks resulted in excessive compaction and higher density. Consequently, the density of plates produced during process development and production in FY 2010 were higher than desirable

The vacuum molding system will be modified in early FY 2011 to incorporate a vacuum regulator and/or vacuum relief valve for complete control of vacuum levels during dewatering. Vacuum levels will be measured at the vacuum manifold throughout the process.

2.1.3 CBCF Production

Sixteen additional prime candidate CBCF insulator sets were produced in FY 2010 to support future RPS Program missions. Qualification of these insulators will be completed in FY 2011. An additional lot of CBCF discs was produced to complete the FY 2009 production commitment. These discs exceeded the density requirement of the specification. Additional work will be performed in FY 2011 to established better control of density for CBCF plates. Numerous Quality Assurance (QA) Surveillances were conducted at ORNL including: instrument calibration, dimensional inspection of insulators, personnel training, and various production activities.

2.1.4 CBCF Qualification

As noted above, the CBCF discs produced to complete the FY 2009 production commitment met the specification with the exception of density. Qualification of three CBCF sleeve lots E43, E44 and E45 produced in FY 2009 was completed. All met the requirements of the specification. With commissioning of the new Flashline™ Thermal Diffusivity Measuring System for the determination of thermal conductivity, Durez 22352 Resin Lot 18FF6095 procured in FY 2008 was finally qualified for prime production. This resin lot was used for all production development and prime production in FY 2010.

2.1.5 CBCF Production and Qualification Procedures

Two CBCF Production Procedures and two Qualification Procedures were revised including the following:

MET-CER-SOP-30, Slurry Preparation

MET-CER-SOP-31, Vacuum Molding

MET-CER-TS-48, Inspection of CBCF Insulators

Y50-AC-65-2325, Determination of Sulfur in Graphite or Carbon by LECO Analyzer

2.1.6 CBCF Production and Qualification Capability

Key personnel including the task manager, two principal technicians and two machinists remain committed to the near-term (~5 years) production of CBCF insulators. A back-up inspector is in training in the dimensional and visual inspection of CBCF insulators and qualification specimens. Additionally, personnel involved in qualification testing will be available to support near-term production.

Facilities and equipment used for the production of CBCF are being upgraded. A new proportional-integral-derivative controller, flow meter, flow control valve and valve controller were installed on the vacuum molding system. Extensive testing was undertaken to establish desired operating parameters for CBCF production as discussed in Section 2.1.2. Additional physical refinements to the vacuum molding system will be made in FY 2011.

The high vacuum furnace used for outgassing CBCF qualification specimens has remained operational through continuous maintenance and calibrations. This furnace has been in service for more than thirty years. A request for capital equipment for a new vacuum furnace was funded in FY 2010. A specification was developed for an oil-free, ultra-high vacuum furnace that will employ a turbomolecular pump to achieve a vacuum of better than 10^{-7} torr at the 1500°C outgassing temperature. The purchase specification will be released in early FY 2011 to solicit competitive proposals from at least three furnace companies.

2.2 IRIDIUM ALLOY BLANK AND FOIL PRODUCTION

The goals for this task are to produce prime blanks and foil under full configuration control, maintain production capability and to supply materials needed for CVS demonstration and maintenance activities. During FY 2010 a total of 12 blanks from the K3 ingot were produced and stored with an approved data package. An upgraded control system and a replacement water-cooling system were installed for the electron-beam melter (EBM).

2.2.1 Blank Production

Melting and extrusion of the K3 ingot were performed during FY 2005. Rolling of the material to sheet was completed in FY 2006. Five of the 17 sheets were processed in FY 2008 to produce 30 blanks. Two additional sheets were processed in FY 2009 to produce 12 blanks. An additional two sheets were processed in FY 2010 to produce blanks. A total of

13 blanks were electro-discharge machined (EDM) from sheets K3-8 and K3-9 and surface ground. All of the blanks passed dimensional and ultrasonic inspection. Twelve blanks passed dye penetrant inspection. One blank showed indications of defects and was deemed not suitable for reworking. A non-conformance report was issued and the blank was designated for use in tensile impact testing. Three of the remaining twelve blanks showed indications of inclusions in the visual examination. These blanks were reworked by sanding in accordance with approved procedures. Subsequent dye penetrant and visual inspections showed all three blanks to be acceptable. The results of chemical and metallographic analyses were acceptable and in the normal range. A data package was prepared for the 12 prime blanks. The blanks were placed in storage with the approved data package in August 2010.

2.2.2 Powder Processing

Blending and preparation of "batch-blends" for the M-batch, containing 80 kg iridium powder, was completed. This included blending and weighing of -100 mesh iridium powder from 14 jars to yield 28 batch-blends of about 2.87 kg each. The powder was processed in accordance with Procedure MET-MatP-SOP-72 Rev.10, operation 3. The powder was stored for future blank and foil production.

Screening of candidate frit vent powder was performed using four jars with a total weight of 14 kg. The screening, performed in accordance with Procedure MET-MatP-SOP-109 Rev. 3. Operation 1 yielded 670 g of powder with the specified mesh size. The candidate powder was stored for further processing when needed. The remaining powder was processed with the above-described M-batch powder for use in blank and foil manufacture.

2.2.3 Major Equipment- Maintenance and Purchase

Installation of the replacement water-cooling system for the electron-beam melting furnace (Fig. 1) was completed. The new system replaced a 20-year old system that could no longer be repaired. This equipment was purchased with FY 2009 capital funds.

The upgraded vacuum and beam emission control systems for the EBM furnace (Fig. 2) were successfully acceptance tested in accordance with the purchase specification for this equipment. The furnace was operated and iridium alloy scrap materials were melted. The system was purchased with FY 2009 capital funds.

A purchase order was placed for a furnace to preheat iridium alloy billets for extrusion. The furnace is to provide an alternative to the existing furnace purchased in 1994, which is now no longer reliable for use in iridium alloy billet heating. The new furnace is to be purchased with FY 2010 capital funds.

Biannual maintenance activities on the 1200-ton extrusion press were completed. The press was returned to normal operation.

A repair of the tungsten hot zone was completed for an alternate vacuum-annealing furnace used for iridium materials

2.2.4 Training

A second technician was trained in the procedures for sampling and cleaning of blanks and reworking of blanks.

Two technicians were trained in operation of the EBM furnace including the new vacuum and beam emission control systems.

A second technician was trained in the procedure for recycling of iridium material.

A second machinist was trained in the procedures for electro-discharge machining of blanks, grinding of blanks, and reworking of blanks by sanding. The training was performed using non-prime sheet to produce 6 blanks. A second machinist was trained in the procedure for surface grinding of iridium alloy ingots. The training was performed using the non-prime ingot RS-17.

2.2.5 Material Characterization

2.2.5.1 Weldability Testing

Characterization of hot cracking during welding has been performed using the Sigmajig test. The test determines the maximum applied tensile stress at which a standard weld can be made without weld line separation. The test equipment was returned to use after an extended period of inactivity. Testing was performed on blanks of iridium alloy scrap material from sheet RS15-6. Tests on five blanks at increasing applied stresses of 100 MPa (14 ksi) up to 155 MPa (22 ksi) resulted in failure only at the highest stress and a measured threshold cracking stress of 140 MPa (20 ksi). This compares with a range of 70 MPa (10 ksi) to 210 MPa (30 ksi) for all DOP-26 alloy production material over the past 20 years.

2.2.5.2 Impurity Effects

Four small ingots of DOP-26 alloy with controlled additions of tantalum impurities were rolled and heat-treated. The material was provided to the Iridium Alloy Characterization task for evaluation.

2.2.6 Deviation Requests (DR)

The following class II DRs were approved in FY 2010:

DR-Ir-231 revised the procedure MC-198 for dimensional inspection of iridium alloy foil. The changes included the use of a ball micrometer for thickness measurement and a decrease in traverse rate for the measurement of surface roughness by stylus profilometry. Surface roughness measurements of iridium blanks and foil were made using a new stylus profilometer instrument. A total of six traverses were made on each of four blanks and two

foils at speeds of 0.1 mm/s and 0.5 mm/s. The results were compared to previous measurements using the old profilometer at a speed of 3.2 mm/s. The results were found to be in good agreement with no change with traverse speed in the average of the measured maximum surface roughness values.

DR-Ir-232 made changes in both the blank specification GPHS M-185 and the foil specification GPHS-M-186. The changes define more clearly the sampling requirements for carbon and oxygen analysis.

DR-Ir-233 revised the procedure MC-413 for machining and dimensional inspection of iridium alloy blanks. Changes were made in the measurement of surface roughness that are the same as described above for foil.

DR-Ir-234 revised the Procedure MET-MatP-SOP-98 "Iridium Alloy Consumable Electrode Preparation". The revised procedure provided more detailed instructions and minimizes potential for chemical contamination of the alloy.

DR-Ir-235 revised Procedure MET-MatP-SOP-109 "Processing of Iridium Powder for Frit Vents." The instructions for precious metal accounting were deleted and editorial changes were made.

DR-Ir-236 revised Procedure MET-MatP-SOP-78 for preparation of data packages and transfer of blanks and foil. The use of gloves in handling finished blanks was deleted and changes were made in the description of methods for assembling and storing the data package documents.

2.2.7 Publications

A presentation at **TMS 2010 Annual Meeting**, Feb 14-18, 2010, Seattle WA, by E. K. Ohriner, G. B. Ulrich, R. G. Miller, and W. Zhang entitled "Surface Processing of an Iridium Alloy" described analyses performed on data from mechanical scribing and experimental laser surface marking of iridium alloy cups.



Figure 1. Replacement water-cooling system for electron beam melting furnace was installed and made operational.

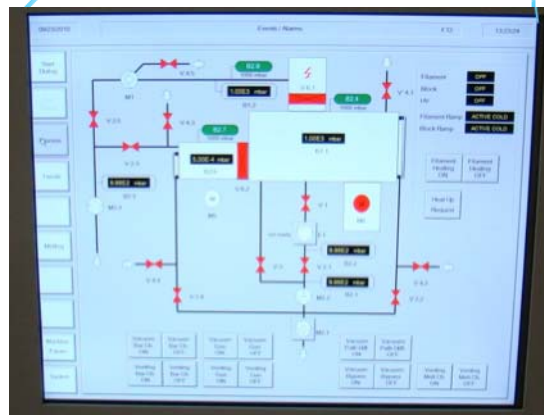


Figure 2. Upgraded vacuum and emission control system for electron beam melting furnace was installed and became operational.

2.3 CLAD VENT SET

2.3.1 Maintenance Production Summary

Three CVS were produced in 2010 as part of the DOE CVS Production Maintenance program. CVS production facility operability was maintained throughout the year. Training of personnel was maintained for all CVS operations during FY 2010. Trend analyses were maintained for all part types. No adverse trends were noted at the end of the year. All six CVS surveillances, per the Surveillance and Process Monitoring Plan for the RPS Program CVS and CBCF Production Tasks, GPHS-QA-002, Revision G (Appendix B), were successfully completed during the year. The CVS surveillances are listed below.

Welding Equipment (Laser and Electron Beam)
Reinspection
Tooling Identification and Control
Measuring and Test Equipment
Instructions, Procedures, and Drawings
Personnel Training

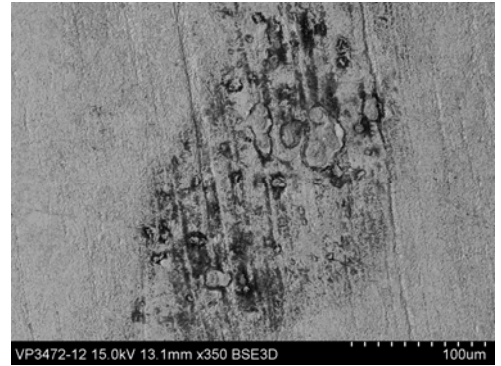
2.3.2 Nonconformance Reports (NCR)

Two nonconformance reports, NCR-CVS-075 and -076 were submitted and accepted in FY 2010. NCR-CVS-075 pertained to an improperly positioned vent hole in cup 3624-05-4379. The vent hole electrical discharge machining fixture, T2D800748A033, Rev. A, was found to provide inadequate positioning repeatability. (Note: two fixtures, T2D800748A033 and AYC790500, were allowed to be used for vent hole machining.) The cup was downgraded to EU and the fixture was removed from production use and scrapped. The procedure, GPHS-XF-3624/25, will be revised in FY 2011 to eliminate reference to this fixture and only fixture AYC790500 will be allowed for vent hole machining.

Shield Cup Assembly 9754-05-5383 was downgraded to EU for a “black spot” in the closure weld zone per NCR-CVS-076. Scanning electron microscopy and energy dispersive spectroscopy indicated that the “black spot” was rich in aluminum oxide along with areas rich in tungsten. Figures 3a through 3h show this “black spot” in a secondary electron image, backscattered electron image, elemental spectra, and X-ray maps of aluminum, carbon, iridium, oxygen, and tungsten, respectively. Most likely this “black spot” was embedded material from the blank grinding/rework operations or cup deburring. At least some of the tungsten is thought to be left over from attempts to remove this “black spot” by probing using a tungsten rod between the air burn-off and vacuum outgas cycles. Screening/evaluation methods or techniques will be developed if this condition becomes recurring.



3a – secondary electron image



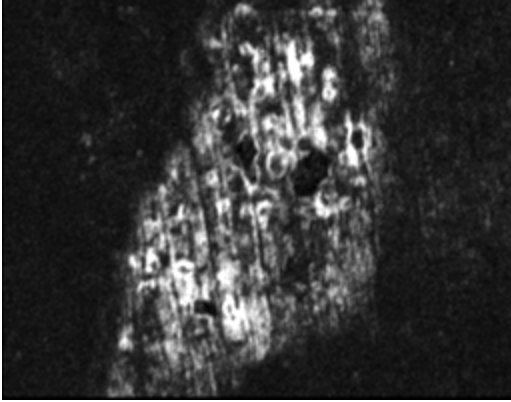
3b – backscattered electron image

Z:\Ulrich\T1269\9450-05-5383\VP3472-12Spc.spc

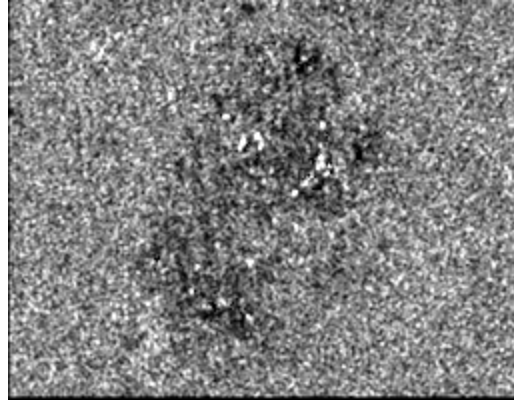
Label A: VP3472-12



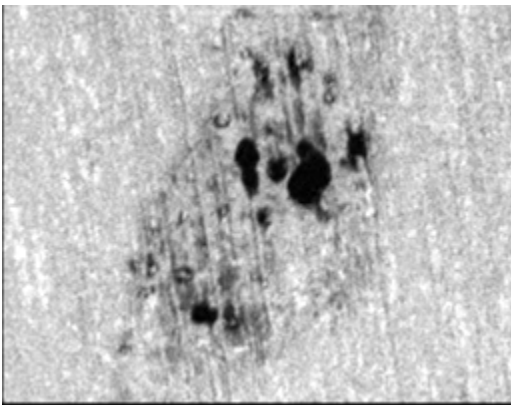
3c – Elemental Spectra



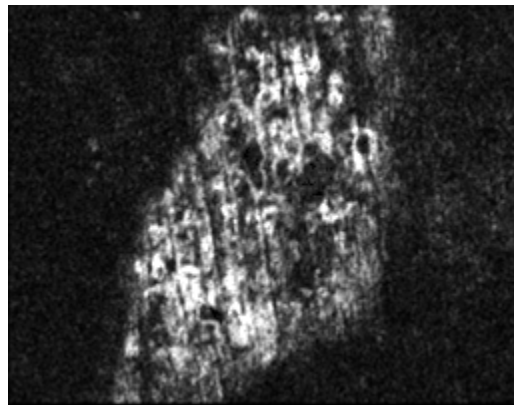
3d - aluminum



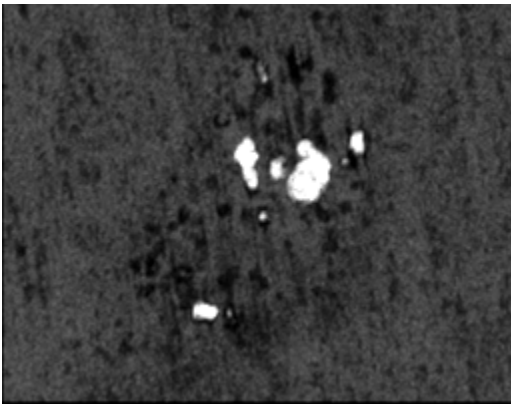
3e - carbon



3f - iridium



3g - oxygen



3h - tungsten

Figure 3. "Black spot" area in the closure weld zone of shield cup assembly 974-05-5383. 3a) secondary electron image, 3b) backscattered electron image, 3c) elemental spectra, 3d-h) x-ray maps of aluminum, carbon, iridium, oxygen, and tungsten.

2.3.3 Deviation Requests

Ten DRs, DR-CVS-080 through -088 and DR-CVS-93, were processed in FY 2010. The revised procedures, their new revision designations, and the procedure titles are listed below in ascending order of their DR numbers.

GPHS-G-9753, Rev. 26 – Vent Cup Assembly
GPHS-G-9754, Rev. 13 – Shield Cup Assembly
GPHS-C-3624/25, Rev. 24 – Cup Dimensional Inspection
GPHS-K-9752, Rev. 14 - Frit Vent Laser Welding
GPHS-K-3620, Rev. 5 – Weld Shield Butt Welding
GPHS-K-9753, Rev. 14 – Frit Vent and Decontamination Cover to Vent Cup Welding
GPHS-XF-3620, Rev. 10 – Weld Shield Fabrication
GPHS-K-001, Rev. 14 – Iridium Alloy Blank Assembly Weld
GPHS-K-9754, Rev. 6 – Weld Shield to Shield Cup Welding
Y50-AC-65-2326, Rev. 0.0 (replaced GPHS-Y-021) – Determination of Carbon in Iridium by Leco Carbon Analyzer

Additional DRs are planned for FY 2011 to update fabrication procedures and the respective tooling drawings.

2.3.4 Evaluation of Aluminum on Iridium

In FY 2009 two of three vent cup assemblies (VCA) were found to have notable black spots on the outside bottom of the cups after completion of the frit vent-to-cup welds. The third VCA had a few small black spot areas on the outside bottom and the inside bottom of the cup. Scanning electron microscopy and energy dispersive x-ray spectroscopy (SEM/EDS) evaluations of these black spot areas on the VCAs and particulates found in the electron beam weld chamber and on the Ten Head Weld Positioner (T2E-140445) tooling showed that all were mostly rich in aluminum. These evaluations indicated that the chamber and the tooling were inadequately cleaned prior to the frit vent-to-cup weld operation and this allowed 6061 aluminum alloy (AA) particulates abraded from the tooling to be circulated in the weld chamber during the pumpdown and backfill cycles.

In FY 2010 certain features of the Ten Head Weld Positioner tooling were re-designed to minimize the generation of particulates in the electron beam welder chamber. These features included changing the Base Plate and End Plate Weldments from 6061 AA to 304L stainless steel. The Pivot Shaft, Bearings, and Positioner Pin were improved to minimize or eliminate sliding contact with the 6061 AA Machine Plate. Also a stainless steel weld chamber slide table was added to minimize sliding contact with the Ten Head Weld Positioner Base Plate. After fabrication and assembly of the modified tooling the CVS Welding Engineer evaluated the tooling for all CVS welds. All of the weld procedures were revised and approved through DRs. The welding personnel were re-trained to the revised procedures with added emphasis on maintaining proper tooling and chamber cleanliness for welding. Maintenance Production components and assemblies were welded successfully.

Also during FY 2010 characterization of the interaction between the 6061 AA particles and the iridium alloy material was completed. Particles were interacted with iridium alloy samples using heat treatments, electron beam welding, and laser welding. [Note: Unsuccessful attempts were made using a Gleeble 3500 System (Dynamic Systems, Inc. – Poestenkill, NY) with direct resistance heating.] The interaction regions were characterized using SEM/EDS, electron probe microanalysis, and/or metallography.

Upon completion of the sample characterization work tensile impact specimens were prepared. Rectangular iridium alloy blanks were electrical discharge machined into tensile impact specimens using molybdenum wire. The edges were deburred and polished. Four specimens, each with one 6061 AA particle of mesh size -100/+270 placed approximately 0.1 inches from the mid-length along the centerline of the width, and four other specimens with no AA particles were vacuum heat treated separately at 1666°C/2 min (Galileo/Ulysses-era re-entry simulation). The specimens were impact tested at the standard 200 feet/second and a temperature of 980°C. All results were well above the 13.5% minimum ductility requirement. Most importantly all eight specimens fractured in the gauge section and none of the fractures were associated with the AA particles. This indicated that 6061 AA particle contaminants do not deleteriously affect the DOP-26 iridium alloy even after exposure to a conservatively plausible re-entry temperature/time.

Since no deleterious effects were found from the study of black spots caused by AA tooling abrasion contamination, silicon powder (99% pure) particles screened to -325/+500 mesh (31 to 44 μm) were placed on two iridium alloy samples (RS12-4-1c and d) as an extreme-worst-case contaminant. [Note: silicon is known to be deleterious to iridium.] Subsequently, the samples were vacuum heat treated separately at the Galileo/Ulysses-era re-entry temperature/time simulation of 1666° C/2 min. Sample RS12-4-1c was examined by SEM/EDS. The areas where particles had been placed were located by SEM, but no silicon was detected by EDS. [Note: the spot size (sampling volume) for EDS is $\sim 1 \mu\text{m}^3$ and the detectability limit is ~ 0.5 w/o.]

Sample RS12-4-1d was metallographically prepared with diamond-only papers with grit sizes of 6, 3, and 1 μm to avoid any additional silicon contamination from the metallographic preparation. The particle/sample interaction areas were identified, and then electron probe microanalysis was performed (using wavelength dispersive spectroscopy – sampling volume of $\sim 1 \mu\text{m}^3$ and a detectability limit of ~ 200 wppm in the counting mode). X-ray maps showed the silicon located at the grain boundaries were only two grains deep or $\sim 70 \mu\text{m}$ into the sample. This potentially-compromised-approximately-70- μm -deep-spot in the bottom of a cup, which still has the starting blank thickness of 630 – 680 μm , leaves the sound cup wall thickness above the specified 550 μm minimum cup wall thickness. Based on these findings and the results from the tensile impact testing, no deleterious effects would be expected for a CVS with “black spots” rich in 6061 AA.

2.3.5 Characterization of Scribed (Engraved) Identity Marks on CVS Cups

CVS cup identity scribe (engrave) marks and styli were evaluated by SEM for eventual comparison to laser marking. Ten diamond-tipped styli were characterized by SEM. The styli base angles (included angle between a horizontal surface and the styli surface leading to the tip) ranged from 18° to 30° . Thus, the styli tip angles ranged from 120° to 144° . The maximum diameters away from the tip of the diamond inserts ranged from $446\ \mu\text{m}$ to $985\ \mu\text{m}$. The height (or depth) of the diamond inserts measured from $74\ \mu\text{m}$ to $279\ \mu\text{m}$. Stylus 1 is shown in Figure 4.

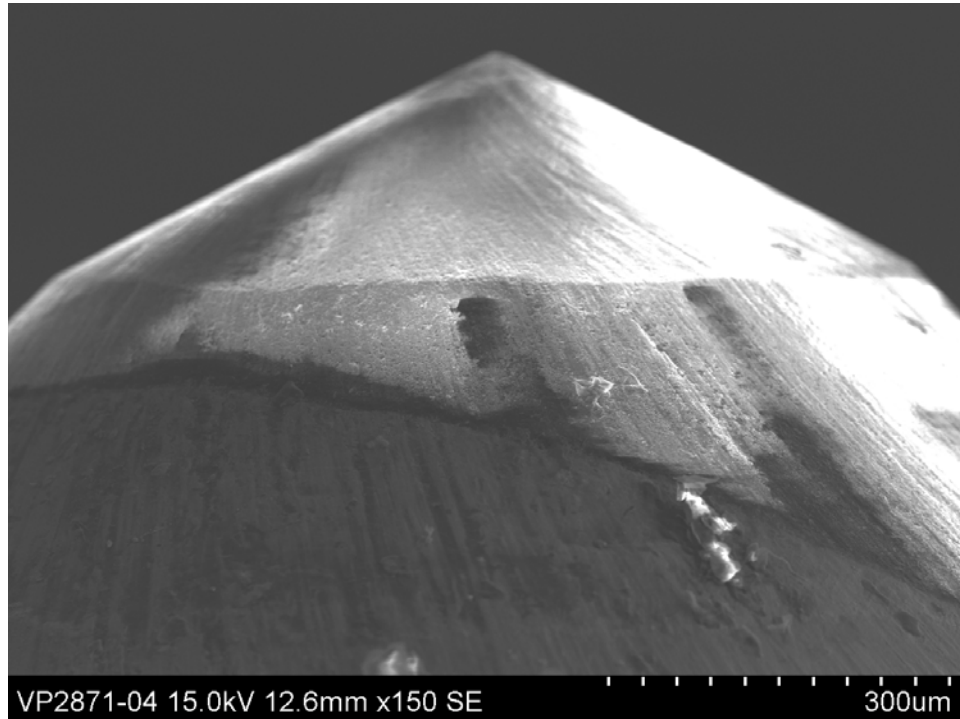


Figure 4. Stylus 1 with diamond tip having 28° base angle, 124° tip entry angle, $765\ \mu\text{m}$ maximum diameter, and $201\ \mu\text{m}$ height.

Nine of these styli were used to scribe a “0” using a $1523\ \text{g}$ load and a “T” using a $435\ \text{g}$ load at the same latitude around the periphery of a recrystallized, but not grit blasted, cup (TC187). The profiles of these scribe marks were measured by SEM typically in 12 locations. The averages of these 12 locations for scribe width and depth plus base and tip entry angles by stylus identity and stylus base and tip entry angles are shown in Table 1 ($1523\ \text{g}$ load) and Table 2 ($435\ \text{g}$ load).

**Table 1. Scribe Data Summary for “0” Scribed with
Nine Styli Using 1523 g Load on Recrystallized Cup TC187**

Stylus ID	Stylus base angle (°)	Stylus tip entry angle (°)	Scribed width (µm)	Scribed depth (µm)	Scribed base angle (°)	Scribed tip entry angle (°)
#1	28	124	88	14	18	144
#2	27	126	89	13	16	148
#3	28	124	83	15	19	141
#4	30	120	84	15	19	141
#5	27	126	82	15	20	140
#6	18	144	91	12	14	152
#7	25	130	87	15	18	143
#8	18	144	89	10	12	156
#9	18	144	92	9	11	158
Av.	24	131	87	13	17	147
S.D.	5	10	4	2	3	7
RSD (%)	20	7	4	18	20	4
Max	30	144	92	15	20	158
Min	18	120	82	9	11	140
Range	12	24	10	6	9	17

**Table 2. Scribe Data Summary for “T” Scribed with
Nine Styli Using 435 g Load on Recrystallized Cup TC187**

Stylus ID	Stylus base angle (°)	Stylus tip entry angle (°)	Scribed width (µm)	Scribed depth (µm)	Scribed base angle (°)	Scribed tip entry angle (°)
#1	28	124	48	7	17	146
#2	27	126	54	7	14	152
#3	28	124	52	9	20	141
#4	30	120	45	7	18	145
#5	27	126	49	8	19	143
#6	18	144	55	6	12	157
#7	25	130	46	6	14	153
#8	18	144	54	4	9	163
#9	18	144	57	5	9	162
Av.	24	131	51	6	14	151
S.D.	5	10	4	2	4	8
RSD (%)	20	7	8	26	28	5
Max	30	144	57	9	19	163
Min	18	120	45	4	9	141
Range	12	24	12	5	11	22

Analyzing and comparing the data (including calculating correlation coefficients) in Tables 1 and 2 indicate that for recrystallized iridium:

- (1) the 1523 g scribe load produces deeper, $\sim 7 \mu\text{m}$, and wider, $\sim 36 \mu\text{m}$, scribe marks than the 435 g scribe load,
- (2) smaller stylus tip entry angles/larger base angles (sharper stylus tips) produce deeper and narrower marks,
- (3) the scribed angles tend to mirror the corresponding stylus angles with correlation coefficients of 0.91,
- (4) scribed tip entry angles are approximately 10° to 20° more (flatter) than the stylus tip entry angles and concomitantly the scribed base angles are approximately 10° less (flatter) than the stylus base angles,
- (5) the scribed base angles for both loads are fairly similar and also the scribed tip entry angles are fairly similar for the two loads, and
- (6) the 435 g load is the better load to use to conform to the specified maximum scribe depth of 0.01 mm ($10 \mu\text{m}$) for recrystallized material.

Figures 5 and 6 show that cracking occurs in the scribe marks with either scribe load in the recrystallized condition. [Note: The 435 g load is used for production scribing of cups.]

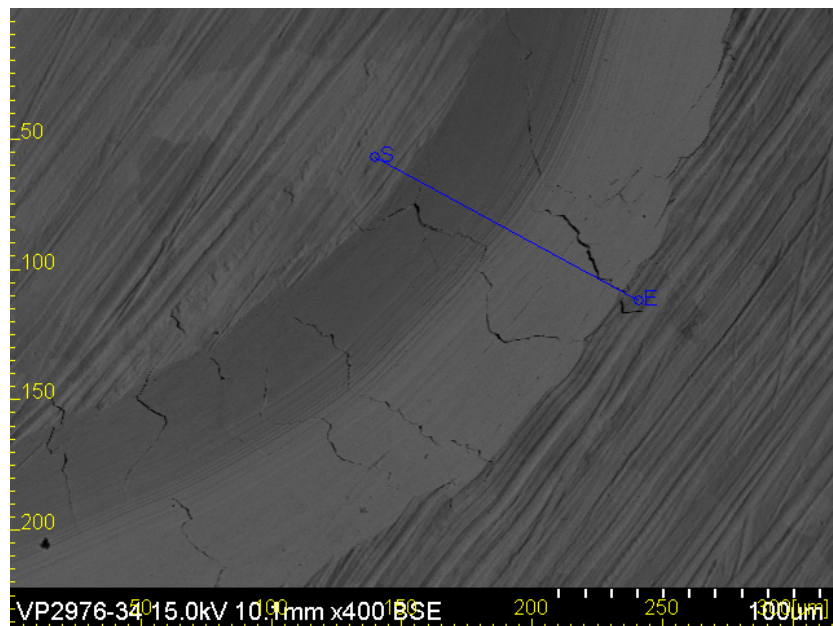


Figure 5. Backscattered electron image showing a typical “0” scribe mark ($92 \mu\text{m}$ wide x $11.4 \mu\text{m}$ deep x 14.1° scribed base or wall angle) using a 1523 g load with surface cracking (tearing) – stylus # 6 on recrystallized Cup TC187.

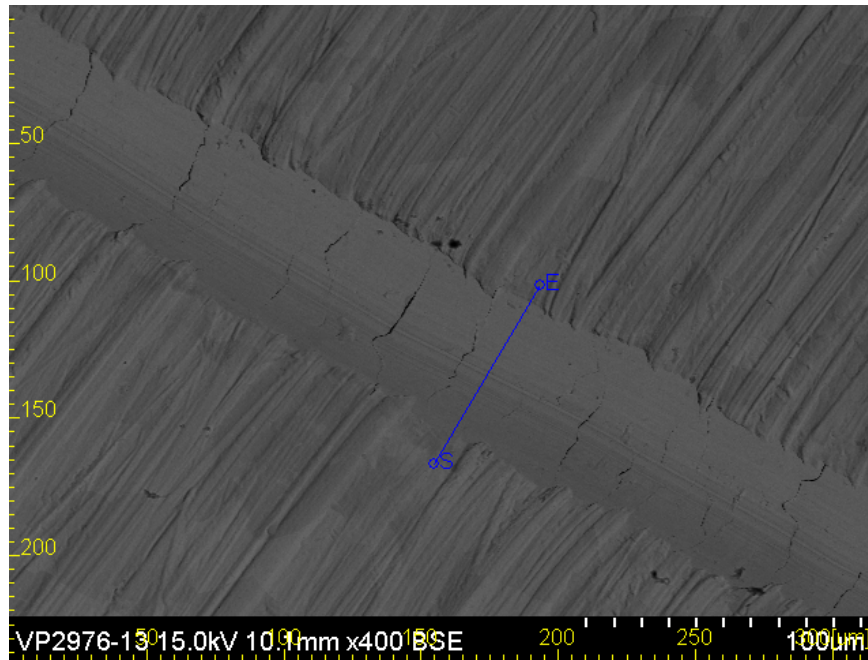


Figure 6. Backscattered electron image showing a typical “T” scribe mark (56 μm wide x 5.6 μm deep x 11.5° scribed base or wall angle) using a 435 g load with surface cracking (tearing) – stylus # 6 on recrystallized cup TC187.

Table 3 summarizes the profiles for three scribe marks or figures, “8”, “C”, and “T”, made on the stress relieved blank RS12-5-4 that was eventually formed into cup TC187. The marks were made using stylus #9 and a load of 1523 g. The marks were measured by SEM in 10 to 12 locations. The averages of these locations for scribe width and depth plus scribed base and tip entry angles are shown in Table 3.

Table 3. Scribe Data Summary for Three Figures Made Using 1523 g Load on Stress Relieved Blank RS12-5-4 (Later Formed to Make Cup TC187)

Stylus ID	Stylus base angle (°)	Stylus tip entry angle (°)	Scribed width (μm)	Scribed depth (μm)	Scribed base angle (°)	Scribed tip entry angle (°)	Scribed Figure
#9	18	144	76	5	7	165	"8"
#9	18	144	80	5	8	165	"C"
#9	18	144	79	5	8	165	"T"

Comparing the data in Tables 1 and 3 for scribe marks made using the same 1523 g load and styli with the same dimensions (18° base angle/144° tip entry angle) indicates that the scribed depths and base angles are notably smaller for the harder stress relieved condition versus the softer recrystallized condition. Concomitantly, the scribed tip entry angles are larger for the stress relieved condition. Also the scribed widths are only mildly narrower for

the stress relieved condition versus the recrystallized condition. Table 3 shows that scribe marks made with the 1523 g load for blanks in the stress relieved condition conform comfortably to the specified maximum scribe depth of 0.01 mm (10 μm).

Figure 7 shows that no cracking occurs in the scribe marks with stress relieved material using a 1523 g scribe load which is the load used for production scribing of blanks.

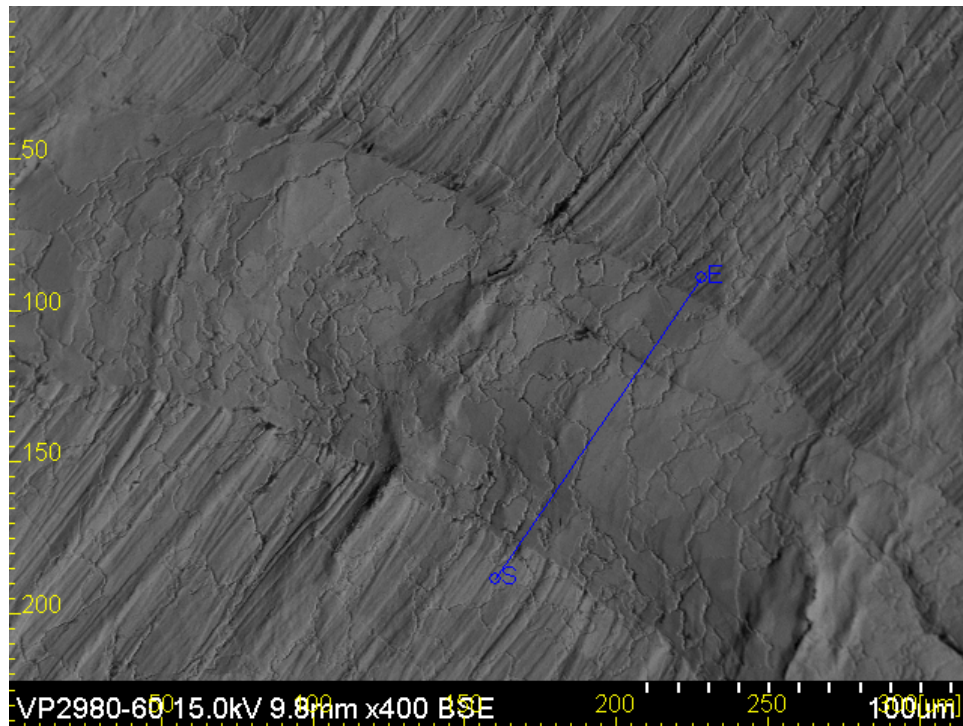
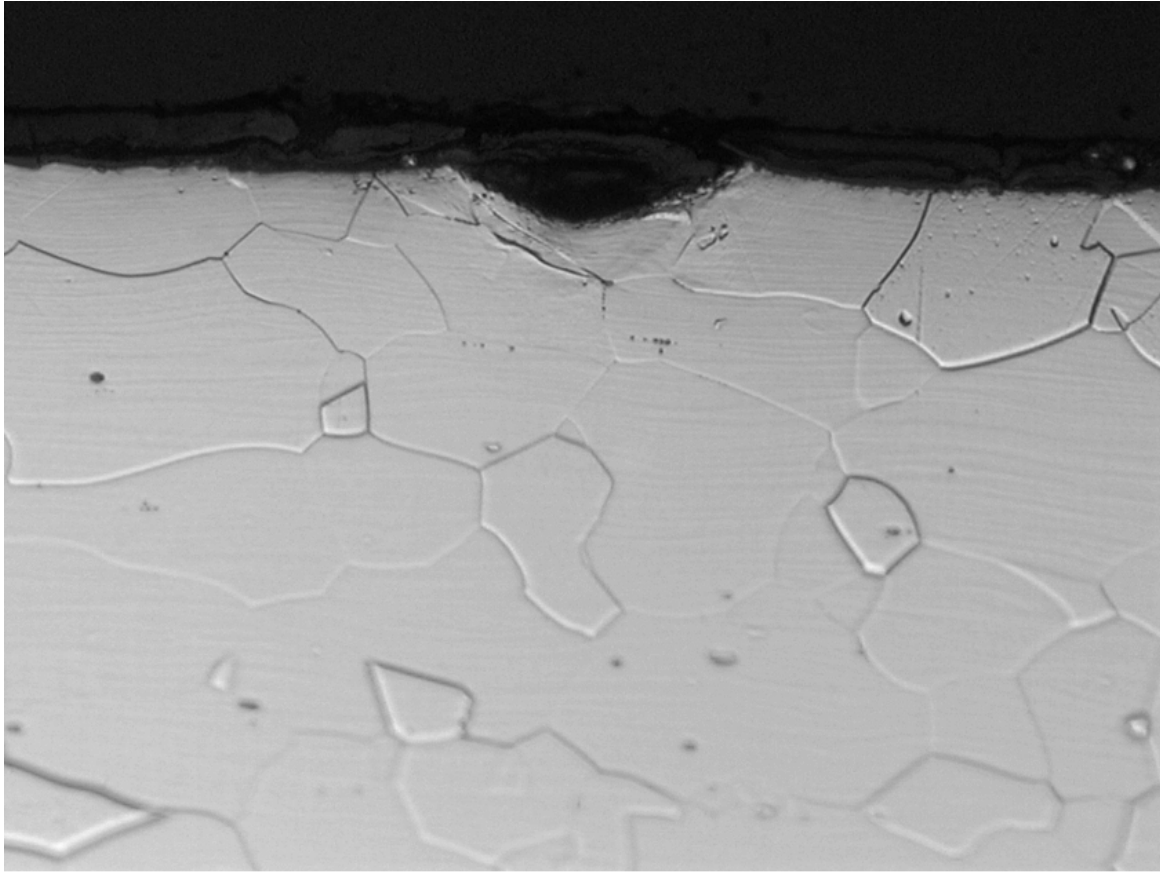


Figure 7. Backscattered electron image showing a typical “8” scribe mark (90 μm wide x 6.5 μm deep x 8.2° scribed base or wall angle) using a 1523 g load with no surface cracking – stylus # 9 on stress relieved blank RS12-5-4 (formed to make cup TC187).

Scribe marks were metallographically evaluated to determine the depth of strain in recrystallized material from loads of 435 g and 1523 g. These evaluations were done for marks from two cups, TC182 and TC187. The strain depths for the 435 g load ranged from 10 – 16 μm while the strain depths for the 1523 g load ranged from 26 – 42 μm . Samples from cup TC187 are shown for the 435 g and 1523 g loads in Figs. 8 and 9, respectively.



10-0267-04

TC-187-1

"T"

500X 10 μ m
100mL HCl+400mL H₂O+
1g NaCl, 2V AC

Figure 8. Metallographically prepared Sample TC187-1 showing cross-section of "T" scribe mark made on recrystallized material using a 435 g load. The depth of strain below the mark is ~14 μ m.

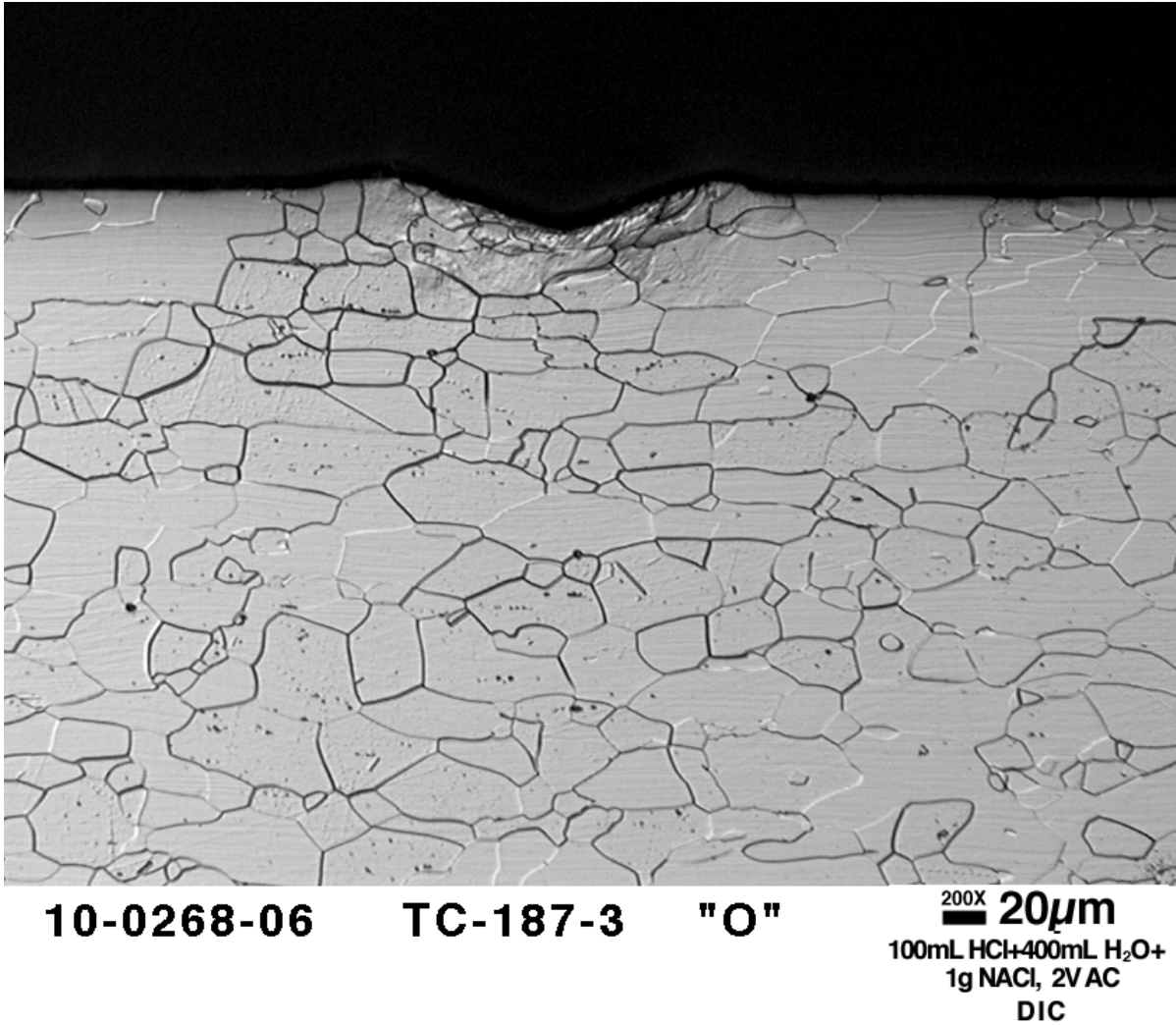


Figure 9. Metallographically prepared Sample TC187-3 showing cross-section of “O” scribe mark made on recrystallized material using a 1523 g load. The depth of strain below the mark is ~42 µm.

Samples with scribe marks made with 435 and 1523 g loads were vacuum heat treated at 1250°C/1 h while an additional sample scribed with a 435 g load was vacuum heat treated at 1500°C/19 h. No abnormal grain growth was noted for any of these samples.

These characterizations of scribed marks on CVS cups may serve as the bases for future comparisons to laser marking.

2.3.6 Decontamination Cover Tooling

A study, begun in FY 2008, to evaluate the potential for improving the decontamination cover blank flattening operation before forming was completed in FY 2010. The original impetus for the study was to produce flatter decontamination cover edges to aid the decontamination cover-to-cup electron beam weld operation. The initial study was halted because of mixed dimensional inspection results for decontamination cover diameters

measured using a micrometer, an Olympus STM comparator/toolmaker's microscope (STM), and a Mitutoyo QVAce 200 vision measuring machine (VMM). Incorporation of tack welding prior to the full circumferential decontamination cover-to-cup weld reduced the impetus for flatter decontamination cover edges. Nevertheless, there was still a need for a fast reliable inspection technique for evaluating parts made from new tooling or after tooling changes. Micrometer measurements are very tedious while the STM measurements are almost as tedious. The VMM is a very fast and repeatable measuring instrument. The expectation was that once the correct inspection parameters were found for the VMM the instrument would be very useful for these types of evaluations.

The VMM inspection parameters for measuring the outside diameter of decontamination covers were selected based on work conducted in FY 2009 and FY 2010. The two Reinspection Surveillance decontamination covers, 3619-01-005 and -015, were inspected to "match" the VMM results as closely as possible to those from the production dimensional inspection Olympus STM. Reinspection data from the last 11 years were used for this matching. VMM inspections were done for each part 10 times and then each part was removed/rotated two more times with 10 inspections after each remove/rotate. The VMM box tool was used in 3 places to find/align the part. Inspections were completed using 1X and 10X magnifications and stage light settings of 7, 8, 10, and 15 with six inspection points. Also six-point VMM inspections were completed using 2X magnification (1X objective and 2X tube lenses) with stage light settings of 7 and 10 plus 6X magnification (1X objective and 6X tube lenses) with a light setting of 23. Twelve-point VMM inspections were done using 1X magnification and stage light settings of 8 and 10 as well as 5X magnification (5X objective and 1X tube lens) and a light setting of 12. The optimum VMM inspection parameters were found to be 1X magnification, stage light setting of 10 utilizing a paper light guard to shield the VMM from external stray light, and 12 inspection points.

The VMM was used in FY 2010 to: (1) select the decontamination cover blanking die and punch diameters for the back-up tooling, (2) evaluate blank flattening loads, and (3) evaluate forming pads made of different materials and hardnesses in order to center the process inspection results for the decontamination cover outside diameter. Decontamination covers were VMM-inspected in the as-blanked, as-flattened, and as-formed conditions. The blanking evaluation indicated that the back-up (#2) tooling dimensions should be the same as those used for the primary (#1) tooling, i.e. punch and die diameters of 0.4572" and 0.4575", respectively. Blank flattening was evaluated using "loads" (ram pressures) of 1000, 2000, 3000, and 4000 psi with one, four and six blanks at a time. No operationally significant differences were found between the flattening loads or the number of blanks flattened at the same time (up to a maximum of six); therefore, the production flattening operation will remain at 1000 psi for a maximum of six blanks. Also no operationally significant differences were found between parts formed using pads made of different materials and hardnesses (rubber with 70A durometer hardness and polyurethane with 90A durometer hardness and also 80A durometer hardness), therefore, the forming pad will remain polyurethane with 75 – 80A durometer hardness.

2.3.7 Cup Sizing and Forming Evaluations Summaries

The current cup production sizing operation is performed at room temperature after the recrystallization operation. The outer surface of a cup is lubricated prior to placing it in a closed steel die. Hydrostatic pressure is applied through a polyurethane punch nose on the inside of the cup to size the cup to the proper final diameter, radius, and roundness dimensions. Cup sizing evaluations in FY 2008 showed that when sizing before recrystallization the wrought (as-formed) cups do not possess enough ductility to achieve proper dimensions. It was decided to continue the sizing load evaluations using recrystallized cups and new sizing punches to determine the practical minimum and maximum sizing load limits. In FY 2009 sizing punches were fabricated from polyurethane stock with durometer readings of 80, 90, and 95 A, then they were dimensionally inspected.

In FY 2010 twenty one recrystallized non-prime test cups were sized and inspected to evaluate the effects of forming parameters used in FY 2008 (Bostik Never-Seez Regular Grade lubricant versus the current Fiske 604 lubricant along with punch and die heating to the current 250°C versus no heating or partial heating [die only or punch only]) and the sizing punches used in FY 2010 on cup dimensions. Extensive statistical summaries and comparisons were completed on dimensional inspection results for forming and sizing involving these cups. The comparisons included cold versus warm forming punches, cold versus warm forming dies, forming lubricants (current Fiske 604 versus Bostik Never-Seez Regular Grade), forming punch-to-die clearances, and polyurethane sizing punch hardnesses (80, 90, and 95 A durometer). In addition to the grouping of the cup dimensional inspection results by the aforementioned parameters the evaluations examined before and after sizing actual values, before and after sizing within-cup-differences, and paired differences (before minus after sizing – both actual and absolute).

The summaries and comparisons showed that within the parameter limits studied the dimensional changes from sizing (cold deformation after recrystallization) could not be reduced. The data also showed tighter dimensional control (less variation) using the 90 and 95 A durometer sizing punches versus the 80 A durometer sizing punch. This information will be useful for modification of the CVS cup fabrication procedure GPHS-XF-3624/25 in FY 2011. These cups will be used as-needed for post-sizing operation training purposes.

2.3.8 Frit Vent Tooling Evaluation

Earlier evaluations of (1) graphites different than the currently-specified UCAR (Clarksburg, WV) ATJ for sintering tooling Pins as well as (2) improved surface finishes on the Pin end faces were unsuccessful in remedying the problem of iridium powder sticking to the Pins instead of the frit vent backing disc during sintering. Re-designs of the sintering tooling were considered with the intent to eliminate contact with the upper iridium powder surfaces and still shield the powder from any disturbances during the vacuum pumpdown. One re-design involved elimination of the Pins by resting a second Spacer with longer graphite dowels on top of the six Bushings. Another re-design used modified diffusion bonding Pressure Pins (0.44" long and 0.315" diameter below the existing 0.62" diameter hemispherical cap) in place of the standard sinter Pins. In FY09 evaluation runs showed that these re-designs yielded acceptable frit vent assemblies, however, they were deemed

“prone to accidentally shifting the sintering Bushing” which disturbs the iridium powder prior to sintering.

Additional Pin designs were fabricated in FY 2010. One design was a further modification of the diffusion bonding Pressure Pins to 0.25” long and 0.315” diameter below a 0.50” diameter hemispherical cap with an overall Pin length of 0.50”. Another design was a modified sintering Pin with 0.5” long sections of 0.310” diameter on both ends with a 0.15” long x 0.5” diameter center section. Both of these are shown in Fig. 10. Unfortunately, these were deemed to have the same shortfall as the previous re-designs, i.e. “prone to accidentally shifting the sintering Bushing”.



Figure 10. Alternate designs for ATJ graphite sintering Pins to avoid contact with iridium frit vent powder during the vacuum sintering operation.

An ATJ graphite Cover was fabricated (see Fig. 11) to be placed over the entire sintering fixture without using Pins. The Cover would shield the iridium powder from any disturbances during the vacuum pumpdown and, without Pins, the Bushings would not be prone to shifting and thus the iridium powder would not be disturbed. Use of the Cover is planned to be evaluated in FY 2011.



Figure 11. ATJ graphite Cover to be placed over a sintering fixture so that Pins would not be required, yet the iridium frit vent powder would be shielded during the vacuum sintering operation.

2.3.9 Metallurgical Destructive Test Sample Evaluations of Recrystallized and Sized Iridium Alloy Clad Vent Set Cup Conditions

Destructive test specimens from cups in three conditions: (1) as-recrystallized (cup TC182), (2) sized + recrystallized (cup TC187), and (3) recrystallized + sized (cup TC177) were metallurgically evaluated. The microhardness results are shown in Table 4. The recrystallized + sized condition, which is the standard order of production processing, showed increased microhardnesses mostly in the radius region, but also in the equatorial region compared to the polar region of the same cup as well as all regions of the other two cup/conditions. The microhardnesses were comparable for all regions of the as-recrystallized and sized + recrystallized conditions. These results indicate that the sizing operation is imparting cold work/strain primarily in the cup radius region and to a lesser extent in the equatorial region. Additional cups will be evaluated in FY 2011 to confirm this.

Table 4. Microhardness Results for Cups in Three Conditions: As-Recrystallized, Sized/Recrystallized, and Recrystallized/Sized

Condition (Cup Identity)	Average Microhardness (HV 1000 gf)		
	Pole	Radius	Equator
As-recrystallized (TC182)	235	233	237
Sized + recrystallized (TC187)	236	236	241
Recrystallized+ sized (TC177)	245	261	249

2.3.10 Miscellaneous Maintenance Production

Cup fabrication (grinding-to-length, lapping, vent notching, electrical discharge machining of vent holes, grit blasting, and scribing) training was started using 10 of 20 existing non-prime cups as well as 13 non-prime blanks. The non-prime blanks were scribed along with the mating waster sheets. The iridium alloy blanks, tantalum barrier disks, and stainless steel waster sheets were cleaned and assembled. They will be used for forming training in FY 2011. Much of this training involves new machinists, Mike Medley and Dianne Bannen. These training sessions were and will continue to be used for procedure verification to determine what changes are needed for a future Vent/Shield Cup Fabrication Procedure GPHS-XF-3624/25 DR, DR-CVS-089. The finished cups will be used for weld set-up and training.

Numerous telephone interviews were conducted during FY 2010 to fill a materials engineer position within the CVS Manufacturing Task. Five of these candidates were brought on-site and interviewed in FY 2010. The search for the appropriate candidate will continue in FY 2011.

The control system for the Lumonics JK 702 laser welder along with the Frit Vent Laser Weld Positioner tooling T2E-140555, Rev. 11 was upgraded in mid-January by PRIMA North America, Laserdyne Systems (Champlin, MN).

Six certified/calibrated Type S thermocouples were received from Furnace Parts, Inc. (Cleveland, OH). These will be used for occasional furnace hot zone checks – independent of the three Type C thermocouples always in each of the CVS high temperature vacuum furnaces. The certification/calibration documents were added to the ORNL Metrology database. The serial numbers assigned by Furnace Parts were used as the ID numbers in the ORNL database (e.g. TC31032). They are in the automated recall system with an interval of 60 months.

The Halmar Electronics, Inc. (Columbus, OH) model DPA1-1230 silicon controlled rectifier power controllers for High Temperature Vacuum Furnaces A and B were replaced with Control Concepts, Inc. (Chanhassen, MN) model 1032A power controllers. Also the Divelbiss Corporation (Fredericktown, OH) Bear Bones Programmable Logic Controller mother boards were replaced for both furnaces. Checkout runs were made for each furnace. These were followed by successful hot zone temperature uniformity evaluations with one new type C thermocouple and two type S thermocouples in each furnace.

2.4 IRIIDIUM POWDER AND INVENTORY MANAGEMENT

The purpose of this work is to manage an iridium inventory for all heat source contractors with emphasis on the significant quantities of iridium located at Los Alamos National Laboratory (LANL), INL, and ORNL and to maintain a no-change iridium inventory through an annual write-off of inventory and processing losses.

2.4.1 Iridium Demand and Supply Schedule

The demand and supply schedule, prepared for contingent planning purposes, presents a strategy to assess the availability of iridium for all improvement and production activities by projecting future demands. An adequate inventory needs to be maintained to meet the needs of the NASA missions and defense missions. Table 5 indicates that enough iridium will be available for these missions.

The first part of the table shows the estimated production demand factors for prime blanks and foil. The schedule of produced blanks and foil represents the quantity and timing for delivery or storage at ORNL. The ingots from new material represent the quantity produced from new iridium powder to make either blanks or foil. These ingots must be produced on a timely basis to meet the lead-time requirement to produce and deliver or store the blanks and foil.

The production of blanks and foil produces recyclable iridium material that can be placed back into the production process at ORNL. A greater economic benefit is realized by using recycled material since the need to purchase powder from an outside vendor is reduced.

Refinable iridium scrap is also generated from the production of blanks and foil. This scrap is sent to a commercial refinery when a sufficient accumulation occurs at ORNL and it makes economic sense based on a comparison of refining costs to that of new material.

Process losses of iridium occur during the working of the material at ORNL, LANL, and INL. Losses also occur during the refining process. These inventory losses are written off annually.

The information contained within the table can be summarized as follows. There will be an adequate supply of iridium powder to produce the hardware for NASA space exploration and defense missions and 99.7 kg will remain at the beginning of FY 2014.

Table 5. Demand and Supply Schedule Shows Factors and Provide Strategy to Ensure an Adequate Supply of Iridium Powder for NASA Space Explorations and Defense Missions

Factors and strategy	U. S. Government fiscal years			
	FY 2010	FY 2011	FY 2012	FY 2013
Production-demand factors				
Produced blanks ¹	10	10	30	30
Ingots from new material	0	0	1	0
Ingots from recyclable material	0	0	0	0
Produced foil (m ²)	0	0	0	0.5
Refining and process losses (kg)				
Refining gain (loss)	0	0	0	0
Processing gain (loss)	(1.4)	(3.0)	(3.0)	(3.0)
Supply strategy (kg) ²				
Beginning balance of powder	120.0	119.7	118.7	100.7
Receipt of refined powder	0	0	0	0
Receipt of purchased powder	0	0	0	0

¹ Estimate of maximum number of blanks

²FY 2014 beginning balance of powder is estimated to be 99.7 kg.

2.4.2 Annual Write-Off

The annual fiscal year 2010 write-off of iridium inventory was completed in May. A total of 4.0 kg of iridium was written off as a normal operating loss. The write-off appropriately reduced the non-fund iridium inventory. This 4.0 kg loss was considered a normal operating loss compared to the history of iridium losses during the past several years.

2.4.3 Iridium Accountability Reviews

The review at ORNL was performed in May. The purpose of this review was to evaluate the accountability, physical inventory, and security of iridium at ORNL. It was concluded that the accountability and security for the iridium was in place and operating in a proper manner. No recommendations were necessary.

The review at LANL was conducted in July. The purpose of this review was to evaluate the accountability, physical inventory, and security of the iridium at LANL. It was concluded that the physical inventory and security for the iridium was in place and operating in a

proper manner. However, the accountability needs improvement. Six (6) recommendations were proposed to enhance the accountability and physical inventory system.

2.5 WELDING

2.5.1 Laser System

The production laser welding system was originally purchased in 1996 and consisted of a three linear axis system and manually controlled rotary axes. The laser is used to weld the frit vent assembly (FVA) cover disc to the backing disc prior to electron beam welding the FVA to the vent cup assembly. The control system used Microsoft DOS as the operating system. A review of the system showed that some components of the system were obsolete and if they failed, replacement components might not be available. FY 2010 capital funding was obtained to modernize the system by updating the computer and operating system to Microsoft Windows and incorporating the rotary axis as a fourth axis in the Computer Numerical Control (CNC) system.

The contract to upgrade the control system and to integrate the rotary weld fixture to CNC control was finalized and released. The contract was placed with Prima North America/Laserdyne. Laserdyne was the original equipment integrator of the welding system. Two production rotary fixtures were sent to Prima North America to integrate them into the CNC system. Figures 12-14 show an external view of the upgraded system, the internal electronic control system upgrade, and rotary fixture modification.

In January 2010 the upgrade was completed by Prima North America/Laserdyne along with system verification and acceptance. A new CNC production welding program was written and verified to perform the FVA laser weld. The standard operating guideline LBW-SOP-GPHS-OP-004, rotary welding fixture drawing T2E-140555, and welding procedure GPHS-K-9752 were updated and approved. Three welding operators were trained and accepted as laser operators for the system. No qualification of the welding parameters was required. Production FVAs were successfully welded following the operator training.



Figure 12. Updated Production Laser Welding System.



Figure 13. New Electronics Upgrade.

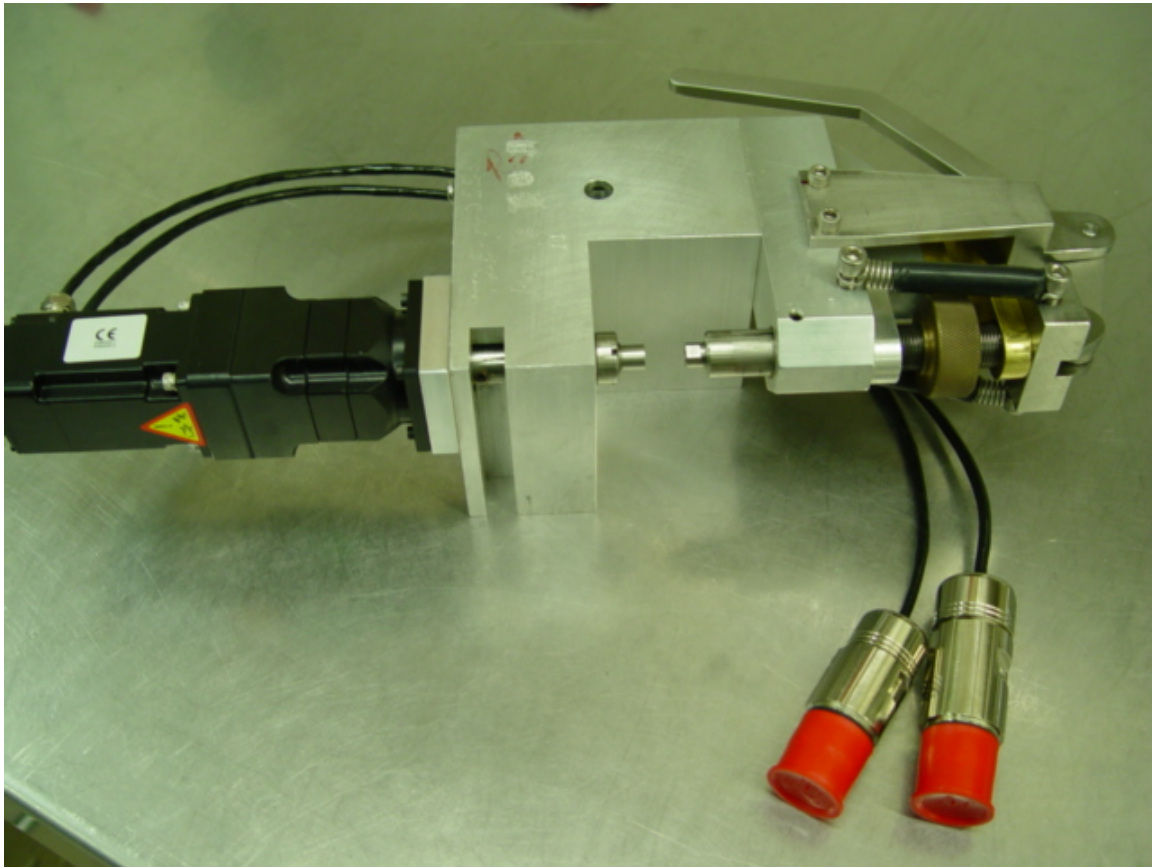


Figure 14. Modified Rotary Positioner.

2.5.2 Electron Beam Welder

The Ten Head Weld Positioner was redesigned and remanufactured during the reporting period. The Positioner had become worn with use and was thought to be responsible for the cracking that occurred while welding a FVA to vent cup assembly in a prior year. The Positioner wear produced aluminum fines that were distributed within the welding chamber during chamber evacuation and back filling. The goal of the redesign was to eliminate aluminum from many components and to engineer sufficient clearances to avoid rubbing where the aluminum was not replaced. Another potential source of metal particles was the constant installation and removal of weld tooling from the welding chamber to load or unload components. A slide table was purchased which would further reduce the generation of metal particles by dramatically reducing the number of times tooling is slid across the weld table.

A standard slide table was purchased from PTR Precision (EBW Manufacturer) with a load rating of five hundred pounds. The installation of the slide table raised the welding location of all electron beam welded components. Beam focus measurements were taken at the new weld heights to determine which procedures required requalification assuming that other existing welding parameters did not require modification. Test results indicated that other welding parameters did not change beyond the allowable ranges permitted by the ASME B&PVC or AWS B2.1. Only the blank assembly weld would need to be requalified due to the weld focus change of greater than five percent of the current value. During these measurements it was also decided to modify the Weld Shield Butt Weld Fixture to minimize the welding height and weld focus change.

Final welding parameter verification was performed on all CVS production electron beam welds after remanufacturing the Ten Head Weld Positioner and the Weld Shield Butt Weld Fixture. Only the beam focus setting was required to be changed for all procedures. As stated previously only the blank assembly weld required requalification. The EBU standard operating guideline GPHS-OP-003 and four welding procedures were revised and approved. Welding procedure GPHS-K-001 and two welding operators were requalified. A qualification report was issued. A typical Blank Assembly weld is shown in Figure 15. This shows the weld cross section between two stainless steel waster sheets used to encapsulate iridium blanks for forming. At least two electron beam welding operators were retrained for all electron beam welding operations. Figure 16 shows the remanufactured Ten Head Weld Positioner installed on the slide table.

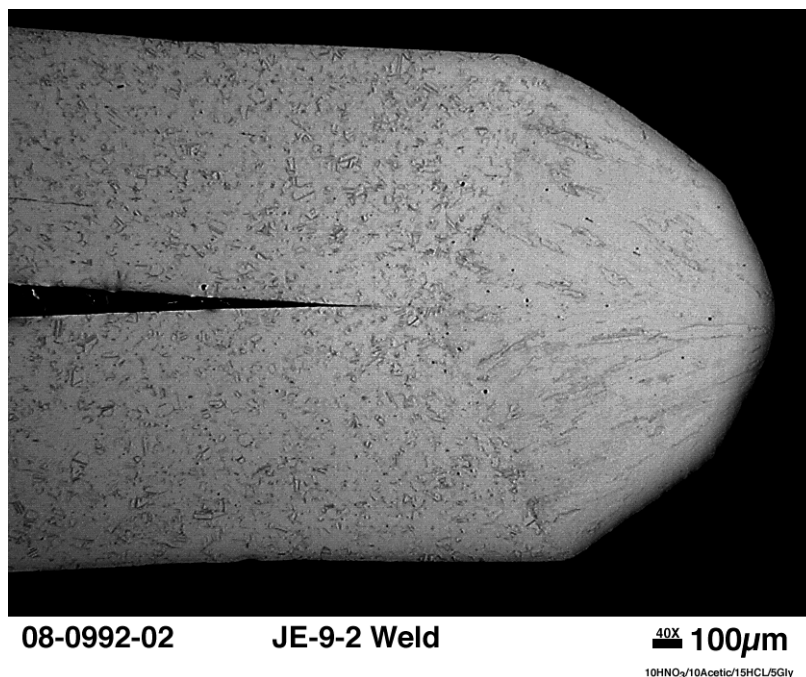


Figure 15. Weld Cross Section Between Two Stainless Steel Waster Sheets Used to Encapsulate an Iridium Blank for Forming.

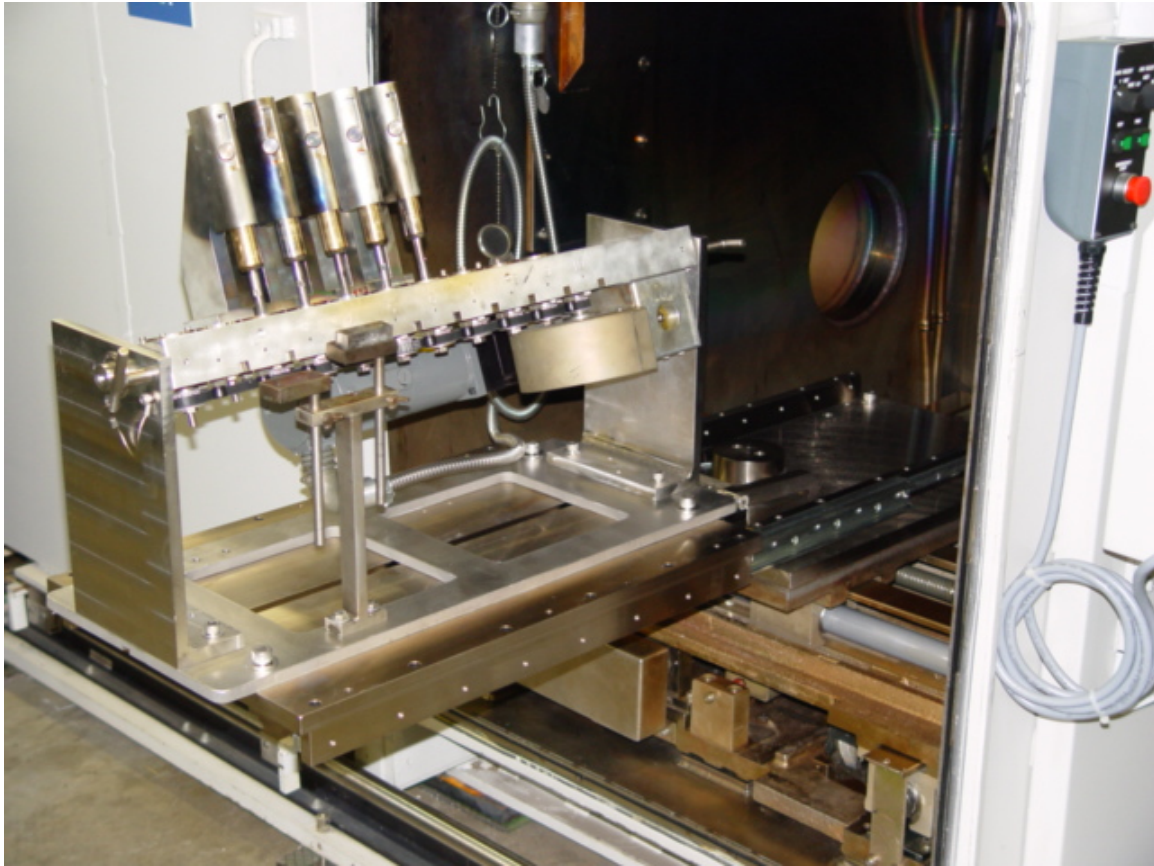


Figure 16. Remanufactured Ten Head Weld Positioner Installed on the Slide Table.

2.5.3 Flow Testing

Long-term testing of a mass flow meter was continued to develop an alternate method of measuring FVA flow rates. The flow meter was coupled to a computer data acquisition system to record data. Further evaluation of flow measurements showed that air contamination could bias mass flow measurements which necessitated extended testing durations. A series of flow measurements were made on three FVAs with the approved method and the mass flow method. Additionally both helium and nitrogen were used as testing gases to determine if an alternate gas may be used with the mass flow meter. These tests were repeated on a monthly basis. Long term testing has shown small differences, generally below 0.3 sccm/min, in the measured flow rate between the two test gases. The variance decreases as the flow rate of an individual FVA increases. Gas flow through the frit appears to be in transitional flow with both molecular and viscous flow components occurring. Further work will be ongoing to further explain and predict the flow rate variance.

3. BASE TECHNOLOGY TASKS

3.1 ALLOY CHARACTERIZATION

In support of the use of DOP-26 iridium as a fuel-cladding material in radioisotope thermoelectric generators (RTG), several studies have been conducted at ORNL to characterize the metallurgical and mechanical properties of DOP-26 iridium. These include measurements of the tensile impact ductility of new process DOP-26 at a high strain rate of $\sim 10^3 \text{ s}^{-1}$ and temperatures of 500-1100°C [1-3]. The tensile impact studies were performed over a range of grain sizes (obtained by heat treating at various temperatures). However, they provided only ductility values (since the tensile impact gun is not instrumented to measure loads at impact strain rates). Therefore, studies using both a servo-hydraulic machine and a screw-driven machine at lower strain rates, up to $\sim 10 \text{ s}^{-1}$, were initiated in 2007 to measure strength and ductility as a function of temperature and grain size [3-5]. Those studies continued during FY 2010 and this report summarizes results of tensile tests performed on DOP-26 iridium at strain rates of 10 s^{-1} and 1 s^{-1} for a grain size of $\sim 40 \text{ }\mu\text{m}$.

Figure 17 shows the stress-strain curves of DOP-26 iridium at temperatures of 25, 400, 600, 750, 900, and 1090°C and a strain rate of 10 s^{-1} . Figure 18 shows the corresponding stress-strain curves obtained at a strain rate of 1 s^{-1} . At both strain rates, the yield strength decreases with increasing temperature. Correspondingly, the ductility (% elongation) increases with increasing temperature. From several previous studies (e.g., ref. [5]) it is known that the increase in ductility with increasing temperature correlates well with increasing amounts of transgranular fracture in DOP-26 iridium. We expect similar behavior in the specimens tested here. Additionally, the ultimate tensile strength (UTS) first increases with increasing temperature, because of the increase in ductility, but then steadily decreases with increasing temperature because the decreasing work hardening rate counteracts the effects of increasing ductility.

Figure 19 compares the temperature dependencies of the mechanical properties of DOP-26 iridium at the two different strain rates investigated in this study. The lower ductilities at the higher strain rate are consistent with earlier results obtained at a smaller grain size. The yield strengths do not change significantly at the strain rates investigated here, which is also consistent with earlier results.

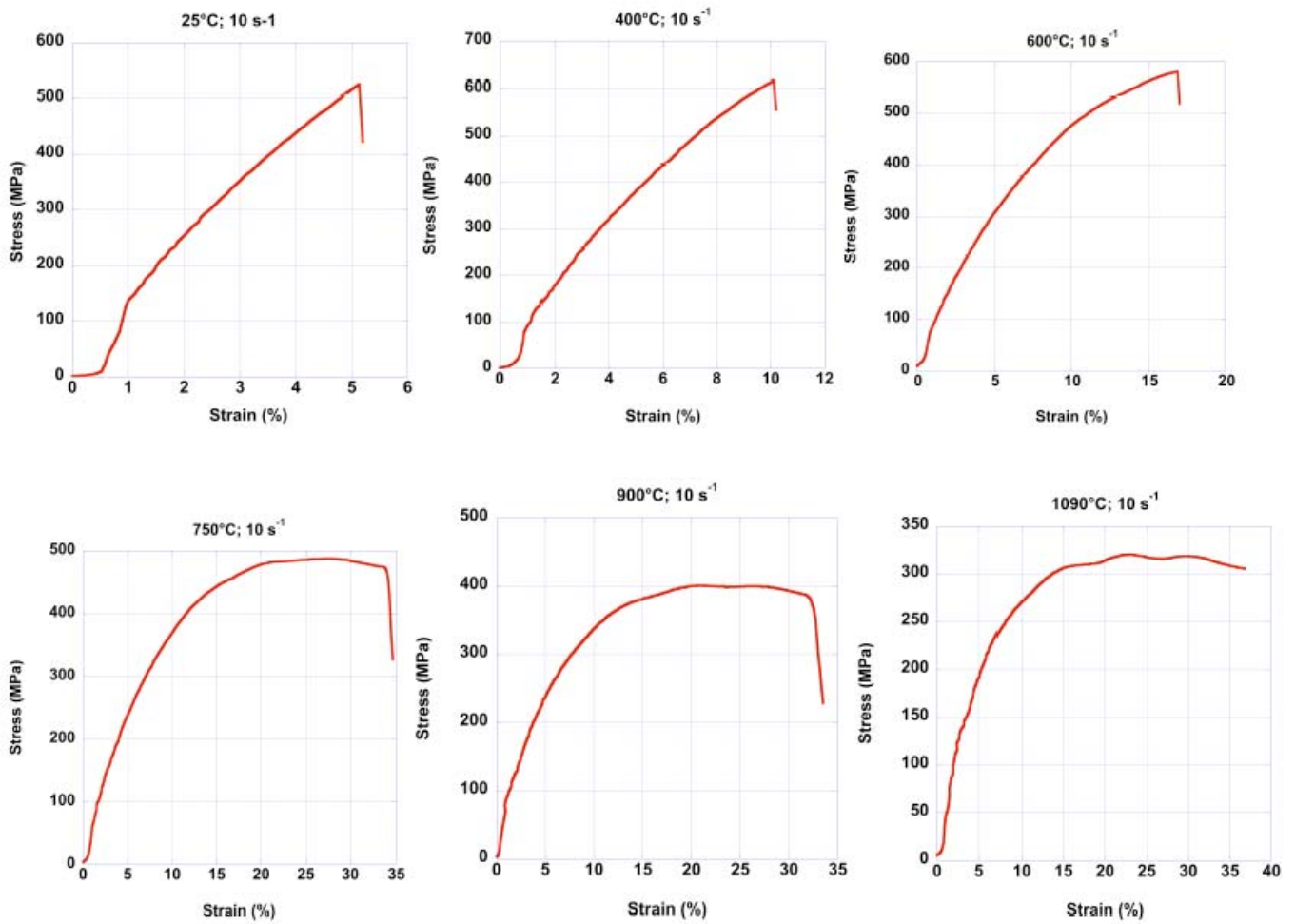


Figure 17. Temperature dependence of the tensile stress-strain curves of DOP-26 iridium at an engineering strain rate of $\sim 10 \text{ s}^{-1}$. The grain size was $\sim 40 \text{ }\mu\text{m}$.

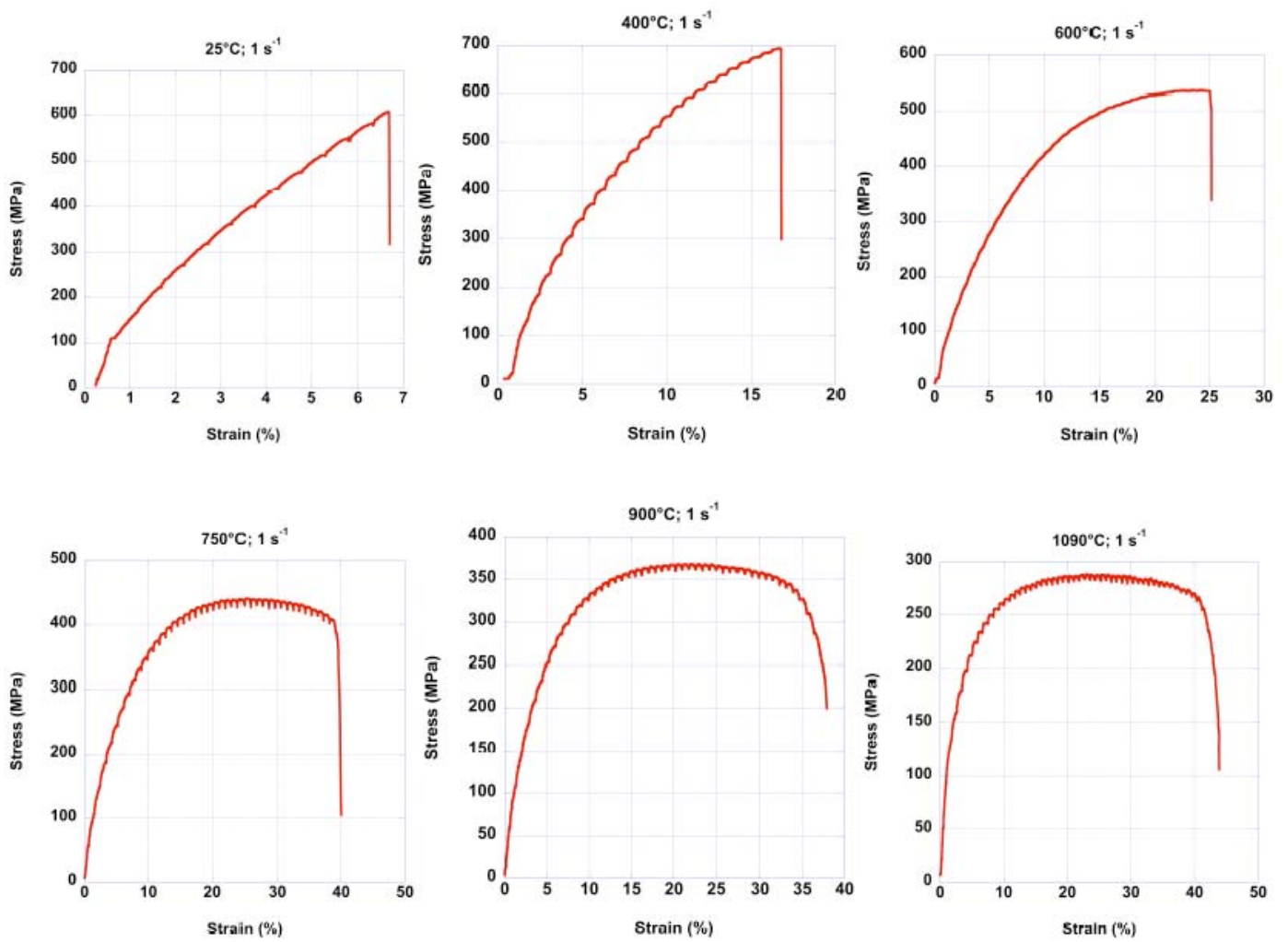


Figure 18. Temperature dependence of the tensile stress-strain curves of DOP-26 iridium at an engineering strain rate of $\sim 1 \text{ s}^{-1}$. The grain size was $\sim 40 \text{ }\mu\text{m}$.

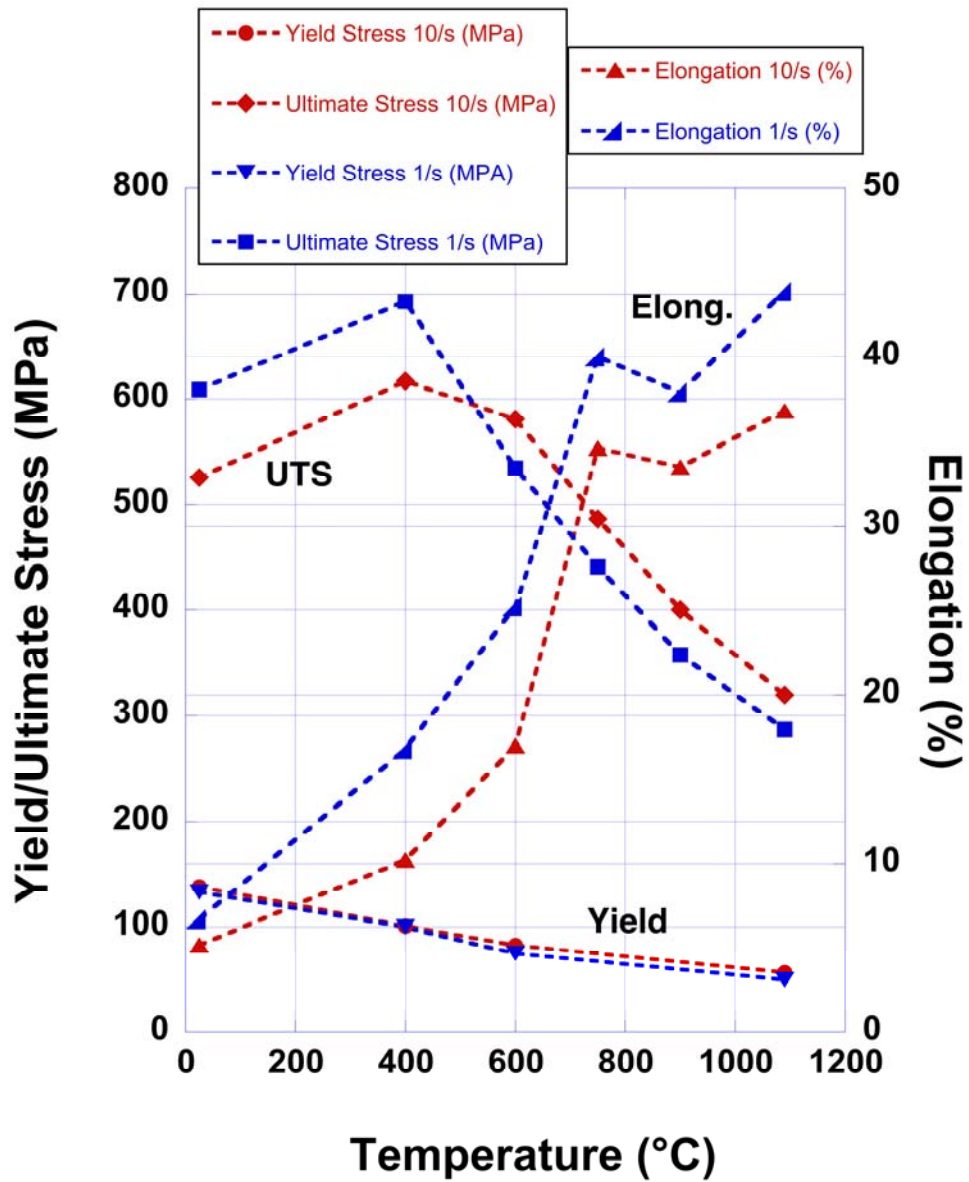


Figure 19. Comparison of the mechanical properties of DOP-26 iridium at two different strain rates of 10 s⁻¹ and 1 s⁻¹.

References

1. C. G. McKamey, A. N. Gubbi, Y. Lin, J. W. Cohron, E. H. Lee, and E. P. George, *Grain Growth Behavior and High-Temperature High-Strain-Rate Tensile Ductility of Iridium Alloy DOP-26*, ORNL-6935, Oak Ridge National Laboratory, Oak Ridge, TN, April 1998.
2. A. Gali, C. A. Carmichael, H. Bei and E. P. George, *Effect of Grain Size on the Low-Temperature (500-900°C) Tensile Impact Ductility of DOP-26 Iridium*, report to DOE-HQ, September 2007.
3. J. H. Schneibel, C. A. Carmichael, and E. P. George, *High Strain Rate Tensile Testing of DOP-26 Iridium*, ORNL/TM-2007/81, Oak Ridge National Laboratory, Oak Ridge, TN, November 2007.
4. J. H. Schneibel, C. A. Carmichael, and E. P. George, *Effects of Temperature, Strain Rate, and Grain Size on the Strength and Ductility of DOP-26 Iridium*, report to DOE-HQ, September 2008.
5. E. P. George, A. Gali, and C. A. Carmichael, *Progress Report on the Effects of Temperature, Strain rate, and Grain Size on the Strength and Ductility of DOP-26 Iridium*, report to DOE-HQ, September 2009.

3.2 ORNL CHARACTERIZATION OF MIN-K TE-1400

3.2.1 Introduction

ORNL was requested to perform additional mechanical testing to further evaluate the mechanical behavior of Min-K 1400 when subjected to a variety of conditions. Min-K 1400 is a high temperature load-bearing fibrous silica insulation that can be used to position, support and insulate an isotopic heat source within some thermoelectric generator housings. Heat source restraint is accomplished by compressively preloading pieces of Min-K between the housing and the heat source. The Min-K 1400 subsequently functions like a spring to store the preload in the form of potential energy, which resists in-line heat source motion and laterally restrains the heat source via friction.

The generator's long-term structural integrity is intimately coupled with preload, since unrestrained heat source motion can damage internal generator components and cripple performance. It is known, however, that Min-K 1400 is susceptible to load relaxation at its anticipated operating conditions. Additionally, complications due to a launch delay have necessitated the performance of additional testing to reduce risk due to unknowns and "soft spots" in currently available test data.

3.2.2 Testing and Results Of Changing Environments Testing

3.2.2.1 Experimental Procedures

Changing environments testing was intended to validate the gradient temperature stress relaxation predictions previously made based on generated data from ORNL^{1,2}. Changes in temperature and strain imparted on Min-K components under gradient temperature conditions were simulated and the effects of these changes were evaluated through testing under various changing environmental conditions.

Testing was performed with an initial temperature gradient of 680/130°C and an initial stress of ≈ 180 psi (1,380 kPa) using 6" (15 cm) diameter, 3" (7.5 cm) long cylindrical samples. Initial load values, changes in temperature and strain for each test, and test durations are shown in Table 6.

Table 6. Changing Environments Test Matrix

(All samples loaded to ≈ 180 psi./1,380 kPa)

Test #	Initial Hot Side (°C)	Initial Cold Side (°C)	Initial Load (lbf./N)	Changes (Temperature, Strain)	Test Duration (hours)
1_1	680	130	5,887/26,187	None	193
1_2	680	130	5,033/22,388	None	820
1_3	680	130	5,162/22,962	600/60°C, +0.72%	3,129
1_4	680	130	5,243/23,322	None	96
1_5	680	130	5,152/22,917	None	1,250
1_6	680	130	5,107/22,717	600/60°C, +0.72% 690/115°C, -0.49%	5,828
1_7	680	130	5,200/23,131	600/60°C, +0.72% 690/115°C, -0.49%	5,253

Following heating of the test sample under a small preload, the sample was loaded to 2.8% strain at a rate of 5.56% strain/hour in four increments with 30 minutes between each load step. The sample was then unloaded at a constant rate, removing the load over ≈ 15 minute period. Data from this preloading experiment was then used to determine the actual loading needed for the specific test specimen to achieve a preload of ≈ 180 psi. Full sample loading was then performed under strain control at a rate of 5.56% strain/hour utilizing a twelve increment loading scheme with three equal steps of load application during each increment. Loading was followed by stress relaxation under strain control for ≈ 75 days. After this period, the first "changing environment" event was performed. While maintaining constant displacement on the test sample (as monitored by the LVDT strain monitoring system), the top and bottom temperatures were changed to 600 and 60°C, respectively. After again allowing the test sample to thermally equilibrate over night, 0.72% strain was applied (using same strain rate as above) in four equal increments spaced 60 minutes apart.

Strain change was then followed by stress relaxation under strain control for ≈ 45 days. After this period, the second “changing environment” event was performed. While again maintaining constant displacement on the test sample (as monitored by the LVDT strain monitoring system), the top and bottom temperatures were changed to 690 and 115°C, respectively. After again allowing the test sample to thermally equilibrate over night, 0.49% strain was applied (using same strain rate as above) in three equal increments spaced 60 minutes apart. Another period of stress relaxation under strain control was then undertaken for a period of at least 20 days.

Transient Strain Events (TSE) expected during actual material service were also simulated using Test #1_6 and Test #1_7. This effort involved three phases of testing. During Phase I of this testing, the strain was raised under displacement control to simulate shell cooling around the Min-K insulation material through a 0.25% increase in strain over a two hour period. The test was then allowed to sit over night under constant displacement. After sitting, Phase II was initiated by decreasing the strain under displacement control to simulate an expansion event through a 0.79% decrease in strain over a 20 minute period. The test was then allowed to again sit over night under constant displacement. Phase III returned the strain back to the original level prior to TSE testing with a target of 0.54% increase in strain applied over a two hour period. Following Phase III, the test was put back under fixed displacement and allowed to relax until the test was terminated.

3.2.2.2 Results

Seven gradient stress relaxation tests were completed under this task with total durations ranging from 240 and 5,765 hours and three tests having “changing environments” events performed on them as shown in Table 6.

Several tests were ended prematurely due to platen or cooling system problems. Figure 20 shows Test #1_3 which was run for a total of 3,129 hours before a failure of the top heater platen occurred. A single “changing environments” test was performed on this sample as shown in Figure. 21. The failure of the top heater platen occurred while attempting to perform the second “changing environments” test. The final stress level (prior to failure of the top platen) was 154 psi (1,062 kPa).

Test #1_6 (shown in Figure 22) was run for a total of 5,828 hours before being ended due to a loss of the cooling water system to the laboratory where the experiment was housed. The first “changing environments” test performed on this sample is shown in Figure 23. The second changing environment event performed on Test #1_6 is shown in Figure 24. After relaxing for 4,125 hours, testing to simulate TSE expected during material service was performed on Test #1_6 as shown in Figure 25. Due to the slow strain rate of these events, ratcheting was experienced by the test frame during the strain application resulting in an increase in the actual strain applied and the time over which the strain was applied.

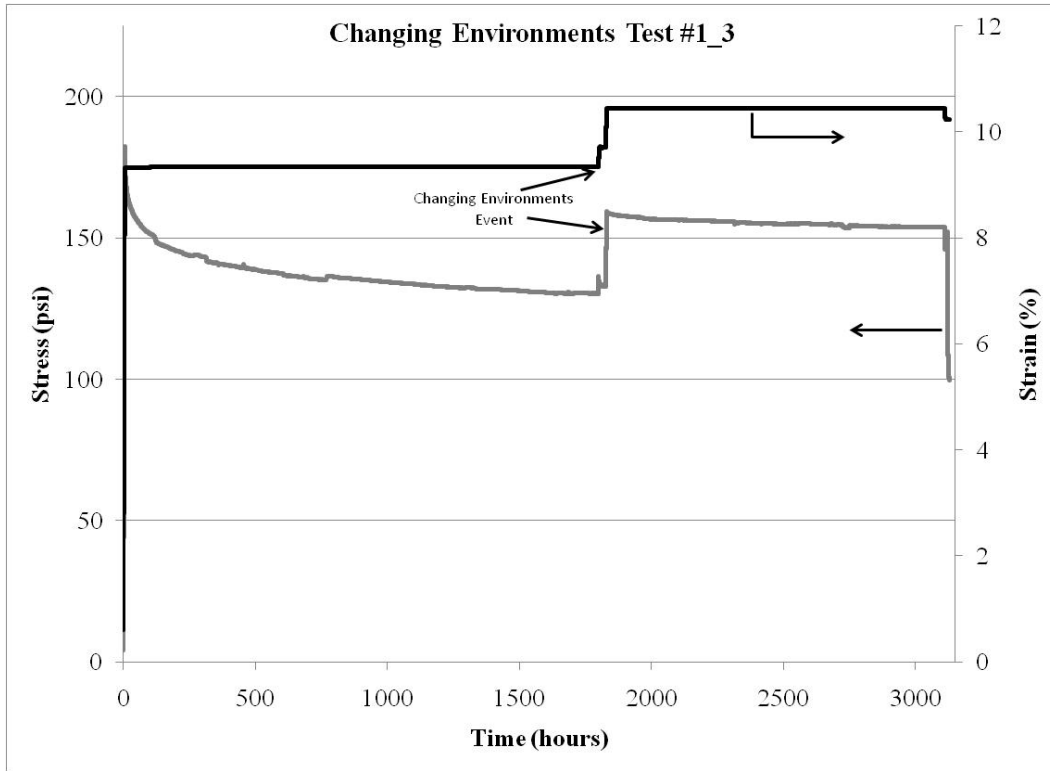


Figure 20. Results from Changing Environments Test #1_3.

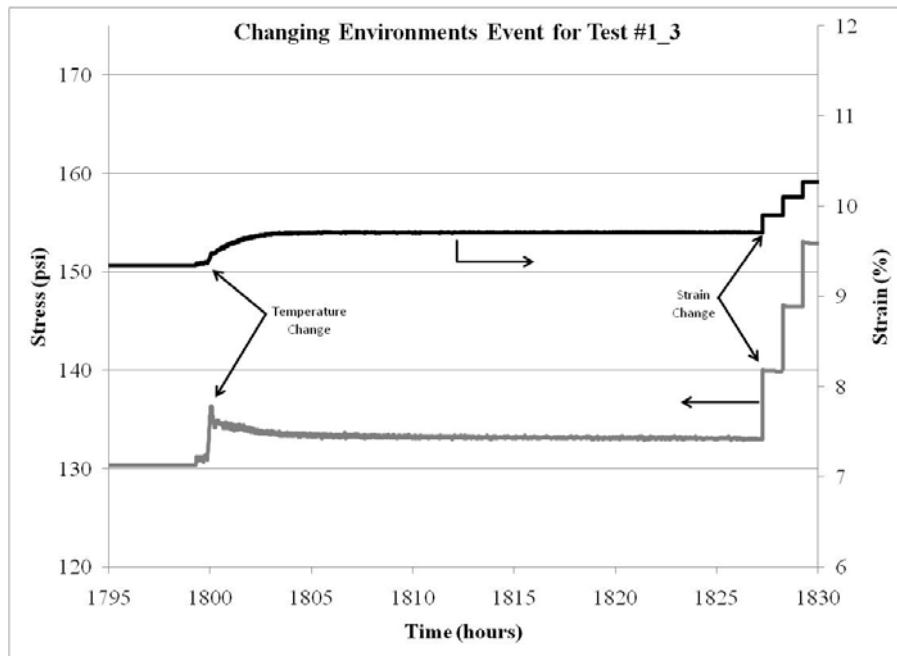


Figure 21. Changing Environment Event for Test #1_3.

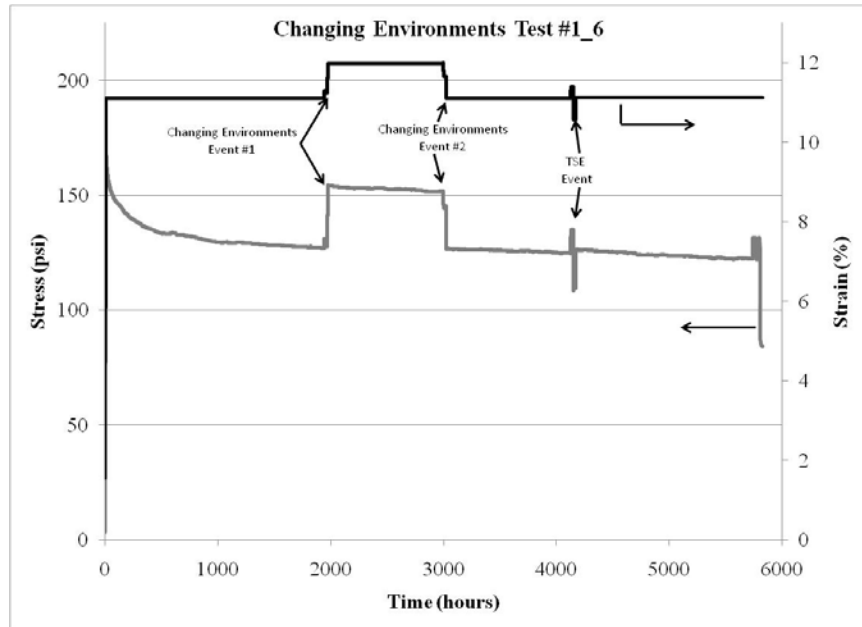


Figure 22. Results from Changing Environments Test #1_6.

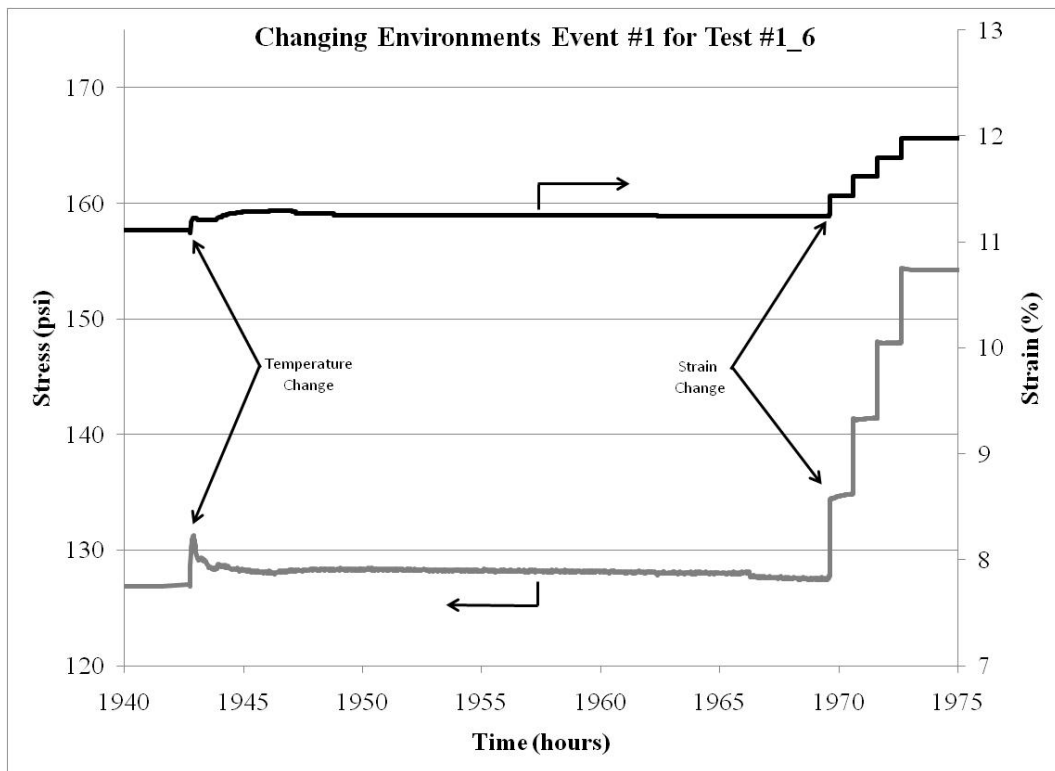


Figure 23. Changing Environment Event One for Test #1_6.

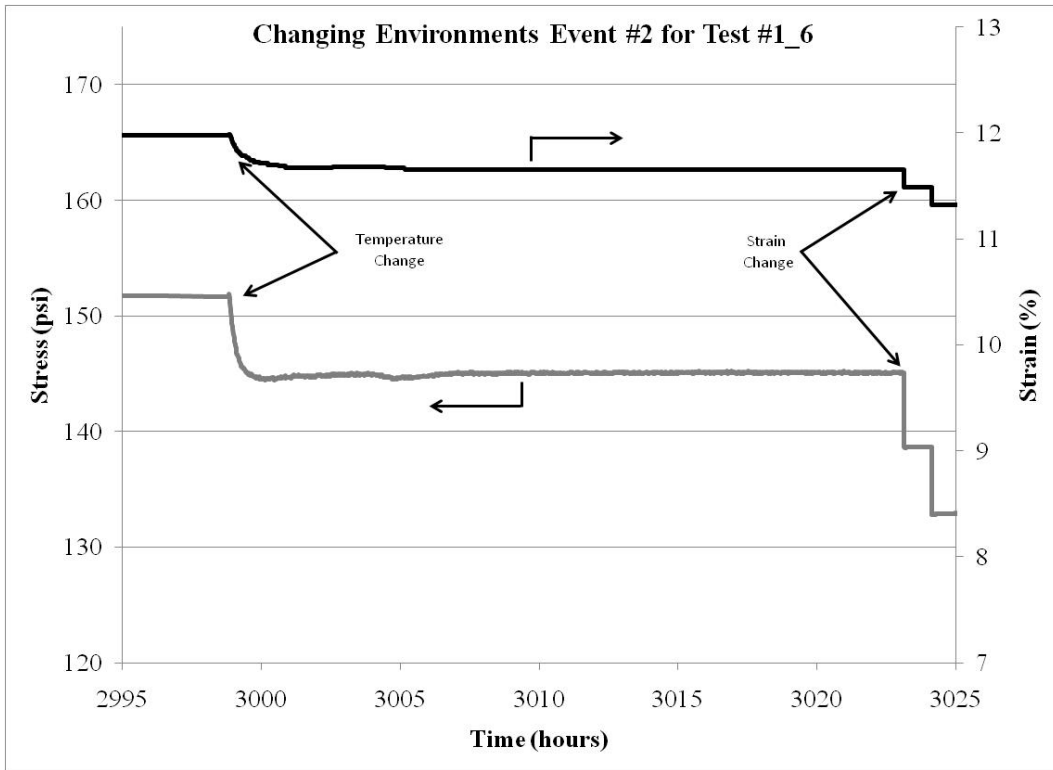


Figure 24. Changing Environment Event Two for Test #1_6.

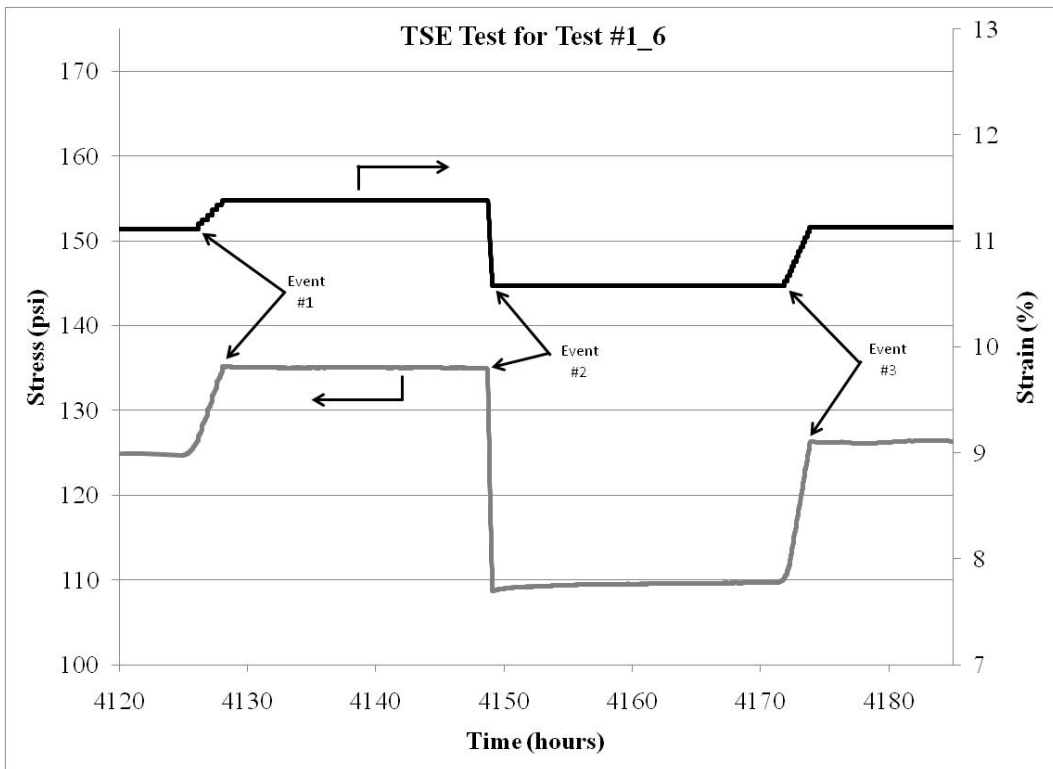


Figure 25. TSE Test for Test #1_6.

Test #1_7 (shown in Figure 26) was run for a total of 5,253 hours before being ended due to the failure of the top platen. The first “changing environments” test performed on this sample is shown in Figure 27. The second changing environment event that was performed on Test #1_7 is shown in Figure 28. After relaxing for 4,118 hours, testing to simulate TSE expected during material service was performed on Test #1_7. Improvements were made in the application of small amounts of strain based on lessons learned during the TSE testing performed during Test #1_6, therefore target strains and times were able to be met.

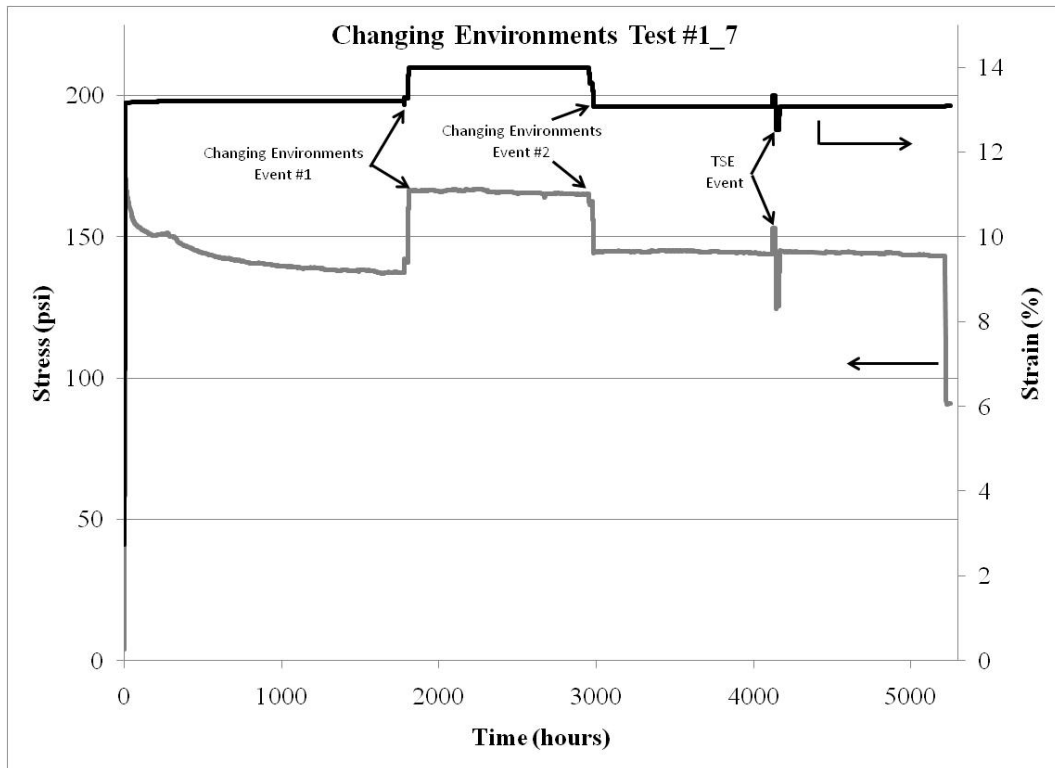


Figure 26. Results from Changing Environments Test #1_7.

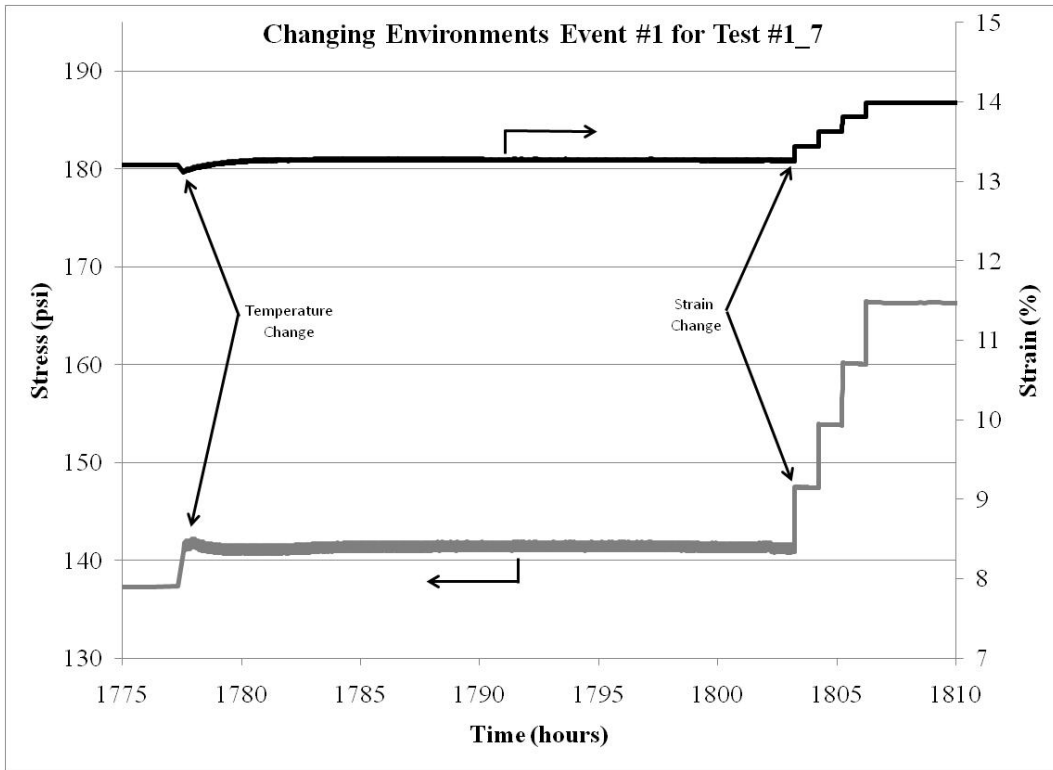


Figure 27. Environment Event One for Test #1_7.

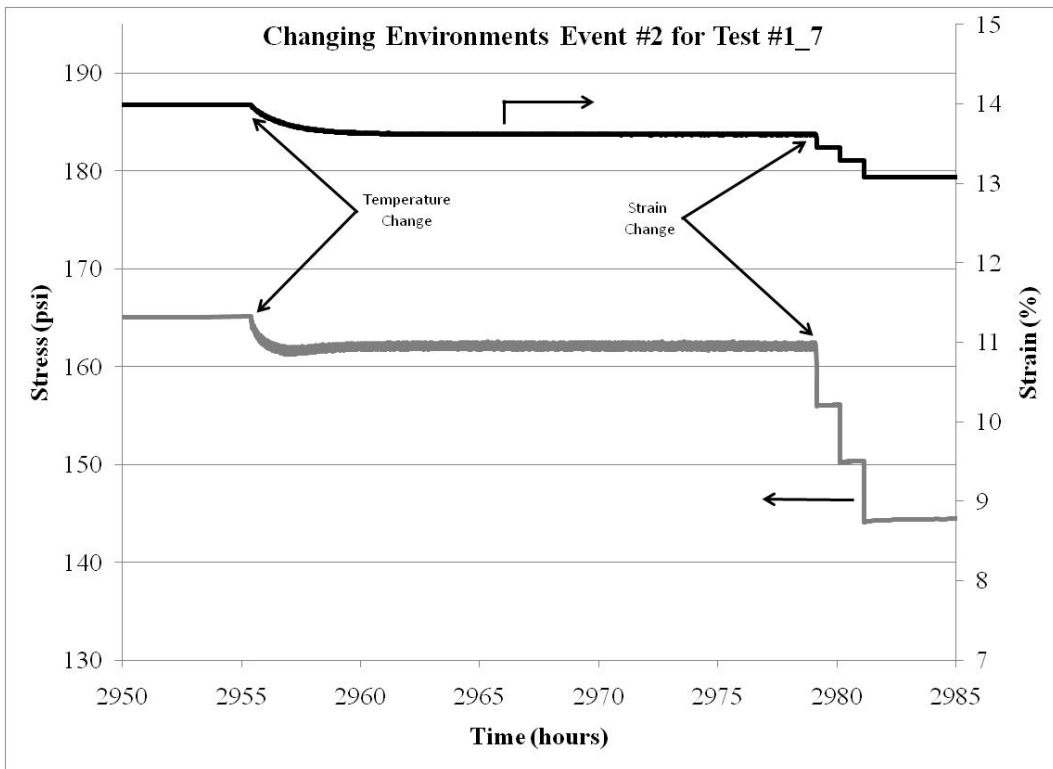


Figure 28. Changing Environment Event Two for Test #1_7.

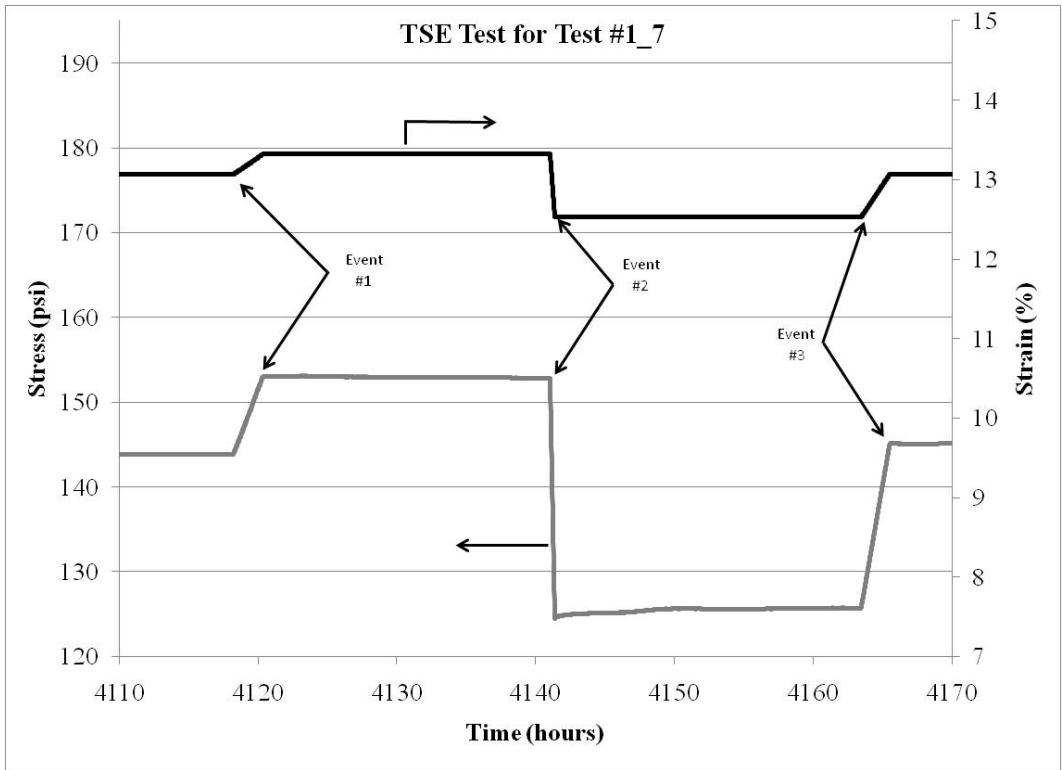


Figure 29. TSE Test for Test #1_7.

3.2.3 Testing and Results of Lateral Load Testing

3.2.3.1 Experimental Procedures

This testing was requested to provide information on the friction created between two pieces of Min-K or a piece of Min-K and a textured aluminum surface at both room temperature and at elevated temperatures. It was found during initial testing at room temperature that the original test set-up did not properly represent the actual intended application of interest for this material, where the Min-K would be in contact with a textured aluminum surface. Therefore, a revised test set-up was constructed. After additional testing, the test set-up was again modified to eliminate lateral loading created by the transfer of forces by a moment arm produced on the rear support of the test system when axial loads were applied to the test assembly. After this modification, initial validation of the test system was performed at room temperature. Elevated temperature testing was performed at 400°C. Replicate testing was performed at both temperatures.

3.2.3.2 Results

Results of initial testing performed at room temperature using the original test set-up are shown in Table 7. This test provided information on the amount of axial stress that the test assembly could accumulate for a specific dead axial load and test speed (speed of actuator to apply lateral load) before slipping between the Min-K layers occurred represented by the maxing out of the measured axial stress. These results were determined to not be

representative of the actual intended application of interest for this material, where the Min-K would be in contact with a textured aluminum surface and not other Min-K. Therefore this test set-up was abandoned after only eight tests.

A matrix of tests performed using the modified test frame is shown in Table 8. Tests #1-10 were performed using the test set-up after the first modification. Figure 30 shows characteristic results from this testing which showed the effect of varying the displacement rate during removal of the axial load. The removal of the axial load at a faster rate resulted in the period of decreased lateral load loss occurring at a higher lateral load value.

Table 7. Initial Lateral Load Testing Results

Small Block (1.5" square)

Test	Weight (kg/lbs.)	Speed (mm/sec.)	Frict. Stress (psi)
1	1/2.2	0.1	1.33
2	1/2.2	0.5	1.19
3	1.75/3.85	0.1	2.88
4	1.75/3.85	0.5	2.92

Large Block (2.5" square)

Test	Weight (kg/lbs.)	Speed (mm/sec.)	Frict. Stress (psi)
5	1/2.2	0.1	0.81
6	1/2.2	0.5	0.72
7	1.75/3.85	0.1	1.32
8	1.75/3.85	0.5	1.52

Table 8. Lateral Load Test Matrix Utilizing Modified Test Frame

Test #	Temperature	Sample Size (inches)	Axial Load (lbs.)	Lateral Load (lbs.)
1 (9/2)	RT	2.25 x 2.25 x 1.0	145	15 unloaded at 0.01 mm/sec
2 (9/2)	RT	2.25 x 2.25 x 1.0	145	15 unloaded at 0.01 mm/sec
3 (9/2)	RT	2.25 x 2.25 x 1.0	250	15 unloaded at 0.01 mm/sec
4 (9/3)	RT	1.0 x 1.0 x 1.0	40	5 unloaded at 0.10 mm/sec
5 (9/3)	RT	1.0 x 1.0 x 1.0	40	5 unloaded at 0.05 mm/sec
6 (9/3)	RT	1.0 x 1.0 x 1.0	65	5 unloaded at 0.10 mm/sec
7 (9/3)	RT	2.25 x 2.25 x 1.0	145	15 unloaded at 0.10 mm/sec
8 (9/8)	RT	2.25 x 2.25 x 1.0	145	25 unloaded at 0.10 mm/sec
9 (9/8)	RT	2.25 x 2.25 x 1.0	145	25 unloaded at 0.10 mm/sec
10 (9/8)	RT	2.25 x 2.25 x 1.0	145	15 unloaded at 0.10 mm/sec
11 (9/22)	RT	2.25 x 2.25 x 1.0	207	25 unloaded at 0.01 mm/sec
12 (9/22)	RT	2.25 x 2.25 x 1.0	188	9 unloaded at 0.01 mm/sec

() indicates test date; RT = room temperature, ET = 400°C

Note: Tests #1-10 performed after first frame modification, Tests #11-61 performed after second frame modification

(Table 8 Continued)

Test #	Temperature	Sample Size (inches)	Axial Load (lbs.)	Lateral Load (lbs.)
13 (9/24)	RT	2.25 x 2.25 x 1.0	188 step loaded	88
14 (9/24)	RT	1.0 x 1.0 x 1.0	28	23 step loaded
15 (9/24)	RT	1.0 x 1.0 x 1.0	28	34 step loaded
16 (9/24)	RT	1.0 x 1.0 x 1.0	20	30 step loaded
17 (10/8)	RT	1.0 x 1.0 x 1.0	65	70 step loaded
18 (10/12)	RT	1.0 x 1.0 x 0.5	65	75 step loaded
19 (10/12)	RT	1.0 x 1.0 x 0.5	65/25	60 step loaded
20 (10/12)	RT	1.0 x 1.0 x 0.5	65	75 step loaded
21 (10/12)	RT	1.0 x 1.0 x 0.5	65	65 step loaded
22 (10/15)	RT	2.25 x 2.25 x 0.5	270	285 step loaded
23 (10/16)	RT	2.25 x 2.25 x 0.5	270	285 step loaded
24 (10/19)	RT	2.25 x 2.25 x 0.5	270	285 step loaded
25 (10/22)	ET	1.0 x 1.0 x 0.5	65	50 step loaded
26 (10/28)	ET	1.0 x 1.0 x 0.5	65/25	75/30 step loaded
27 (10/28)	ET	1.0 x 1.0 x 0.5	65/25/15	75/30 step loaded
28 (11/11)	ET	1.0 x 1.0 x 0.5	65	60 step loaded
29 (11/11)	ET	1.0 x 1.0 x 0.5	65/25	70/50 step loaded
30 (11/11)	ET	1.0 x 1.0 x 0.5	65/25	50 step loaded
31 (11/13)	ET	1.0 x 1.0 x 0.5	65/25	70/50 step loaded
32 (11/13)	ET	1.0 x 1.0 x 0.5	65/25	50 step loaded

() indicates test date; RT = room temperature, ET = 400°C

Note: Tests #1-10 performed after first frame modification, Tests #11-61 performed after second frame modification

(Table 8 Continued)

Test #	Temperature	Sample Size (inches)	Axial Load (lbs.)	Lateral Load (lbs.)
33 (11/16)	ET	1.0 x 1.0 x 0.5	65/15	50 step loaded
34 (11/17)	ET	1.0 x 1.0 x 0.5	65/15	30 step loaded
35 (11/18)	ET	1.0 x 1.0 x 0.5	65/15	30 step loaded
36 (11/20)	ET	1.0 x 1.0 x 0.5	65/25	70/50 step loaded
37 (11/23)	ET	1.0 x 1.0 x 0.5	65/25	30 step loaded
38 (11/25)	ET	1.0 x 1.0 x 0.5	65/15	30 step loaded
39 (11/30)	ET	1.0 x 1.0 x 0.5	65/10	30 step loaded
40 (12/3)	ET	1.0 x 1.0 x 0.5	65	70 unloaded laterally
41 (12/10)	ET	1.0 x 1.0 x 0.5	65/25	50 step loaded
42 (12/11)	ET	1.0 x 1.0 x 0.5	65/15	40 step loaded
43 (12/14)	ET	1.0 x 1.0 x 0.5	65/10	30 step loaded
44 (12/16)	ET	1.0 x 1.0 x 0.25	65/25	70/50 step loaded
45 (12/21)	ET	1.0 x 1.0 x 0.25	65/25	50 step loaded
46 (12/23)	ET	1.0 x 1.0 x 0.25	65/15	40 step loaded
47 (12/29)	RT	1.0 x 1.0 x 0.25	65/25	70/50 step loaded
48 (1/4)	RT	1.0 x 1.0 x 0.25	65	50 step loaded
49 (1/4)	RT	1.0 x 1.0 x 0.25	65/15	40 step loaded
50 (1/5)	RT	1.0 x 1.0 x 0.25	65/15	40 step loaded
51 (1/12)	RT	1.0 x 1.0 x 0.25	65/25	70/60 step loaded
52 (1/12)	RT	1.0 x 1.0 x 0.25	25	50 step loaded

() indicates test date; RT = room temperature, ET = 400°C

Note: Tests #1-10 performed after first frame modification, Tests #11-61 performed after second frame modification

(Table 8 Continued)

Test #	Temperature	Sample Size (inches)	Axial Load (lbs.)	Lateral Load (lbs.)
53 (1/25)	RT	1.0 x 1.0 x 0.25	65/25	70/50 step loaded
54 (1/26)	RT	1.0 x 1.0 x 0.25	65/25	50 step loaded
55 (2/4)	RT	1.0 x 1.0 x 0.25	65/25	40 step loaded
56 (2/4)	RT	1.0 x 1.0 x 0.25	65/25	50 step loaded
57 (3/26)	RT	2.25 x 2.25 x 0.5	152	330 step loaded
58 (3/26)	RT	2.25 x 2.25 x 0.5	152/95	181 step loaded
59 (3/30)	RT	1.0 x 1.0 x 0.5	25/10	30 step loaded
60 (4/15)	RT	1.0 x 1.0 x 0.5	25/15	40 step loaded
61 (4/15)	RT	1.0 x 1.0 x 0.5	35/15	30 step loaded

() indicates test date; RT = room temperature, ET = 400°C

Note: Tests #1-10 performed after first frame modification, Tests #11-61 performed after second frame modification

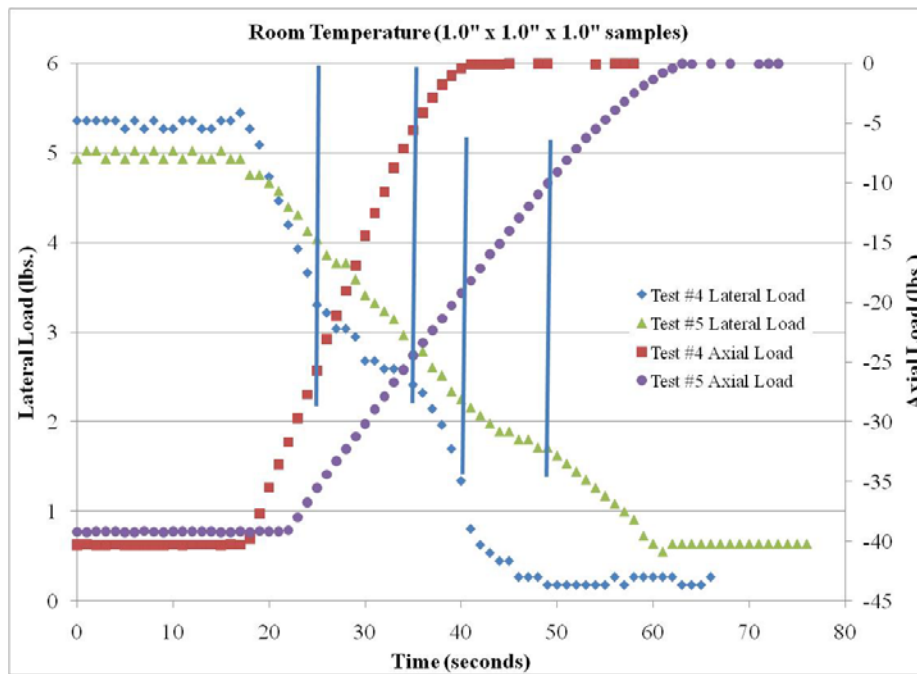


Figure 30. Results for 1" Samples Using Lateral Load Testing Set-Up after First Modification.

To confirm that the loss of lateral load was related to the removal of the axial load and not to some other source, Test #7 was run on a 2.5" square sample which was loaded to 145 lbs. axially and 15lbs. laterally as shown in Figure 31. The axial load was removed from this sample at a constant displacement rate of 0.10 mm/sec with holds when the axial load reached 75 and 45 lbs. As expected, the lateral load stopped decreasing when the axial load was held constant at each of the above values.

Tests #11-61 were performed using the test set-up after the second modification. For Test #11 and 12, the lateral loads were found to decrease rapidly at a constant rate with the removal of the axial load, contrary to the behavior seen in previous testing discussed above. It was decided though that this test method was still not producing the desired data for analysis, therefore the test procedure was again modified.

Subsequent tests were run by axially loading the test sample in a step fashion and observing the corresponding lateral load. After each load step the loads (both axial and lateral) were allowed to relax as the sample was held under constant axial displacement. As shown in Figure 32, it was found that coupling still existed between the axial and lateral loads. This was thought to be due to deflection of the frame push rods. Subsequently, work was done to stiffen the frame by providing supports to the push rods.

Test #17-61 were run after stiffening the test frame. An example of this testing is shown in Figure 33. The behavior exhibited by tests at 400°C was found to be similar to that experienced at room temperature. Tests were also run at 400°C using thinner test samples. Results indicated that sample thickness does not significantly affect material performance in this test.

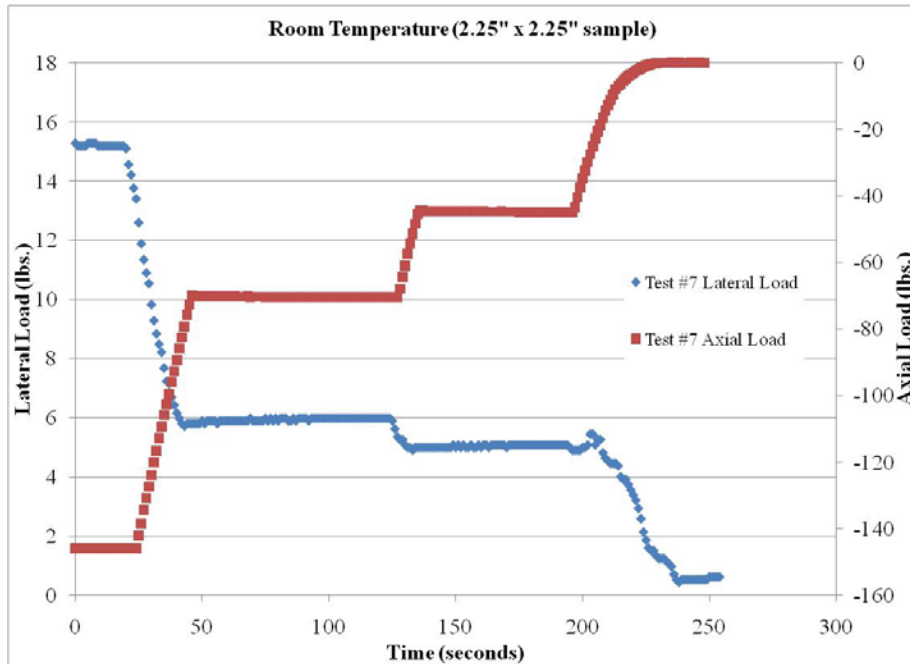


Figure 31. Results for 2.5" Square Sample Using Lateral Load Testing Set-Up after First Modification Using Step Unloading.

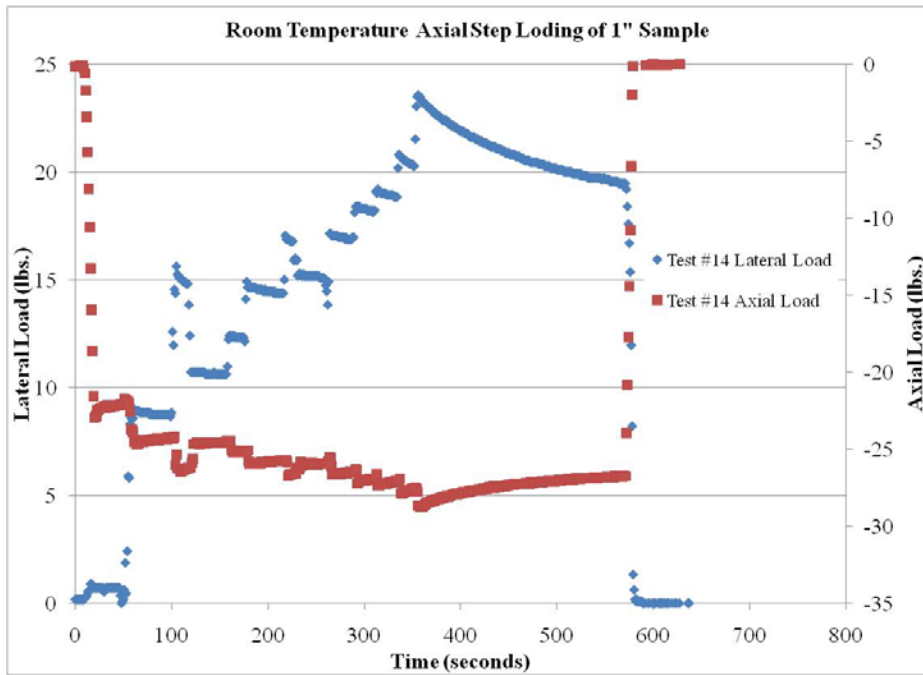


Figure 32. Results for Lateral Step Loading of 1" Square Sample Using Lateral Load Testing Set-Up after Second Modification.

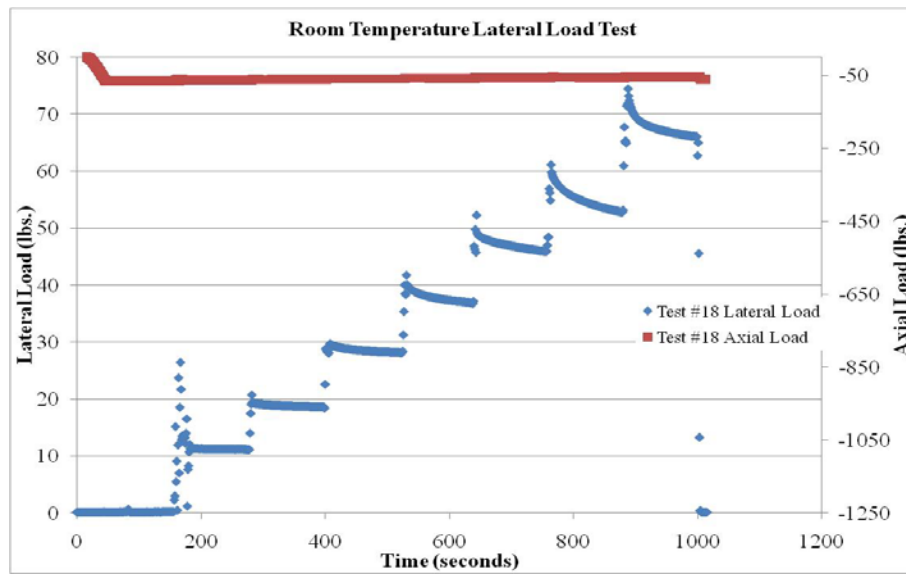


Figure 33. Characteristic Results for Lateral Step Loading of 1" Square Sample Loaded to 65 lbs. Axially.

In summary, results of testing performed using the test set-up after the first modification (Tests #1-10) where samples were loaded axially and then laterally before the axial load was removed at a constant displacement rate showed a decrease in lateral load until a corresponding axial load was reached at which point the lateral load remained constant for a fixed period before the lateral load began to decrease to zero as the remainder of the axial load was removed. There was good repeatability found between repeat tests run under these conditions. Tests run under varying displacement rates during removal of the axial load indicated that the removal of the axial load at a faster rate resulted in the period of decreased lateral load loss occurring at a higher lateral load value. To confirm that the loss of lateral load was related to the removal of the axial load and not to some other source, a test was run which was loaded axially and laterally with the axial load removed at a constant displacement rate and holds when the axial load reached set levels. As expected, the lateral load stopped decreasing when the axial load was held constant at each hold. A test was also run where the axial load was intermittently removed and reapplied at various levels again confirming the direct correlation between the axial and lateral loads, along with an increase in the lateral load with the axial reloading events. This indicated coupling between the axial and lateral loads due to problems with the test fixture which needed to be corrected for improved accuracy of the test data analysis. Therefore, the second modification of the test set-up was undertaken.

Results of testing performed using the test set-up after the second modification (Tests #11-61) showed that the lateral loads decreased rapidly at a constant rate with the removal of the axial load, contrary to the behavior seen in previous testing. It was decided though that this test method was still not producing the desired data for analysis, therefore the test procedure was again modified. The next tests were run by axially loading a sample in a step fashion and observing the corresponding lateral load. After each load step the loads (both axial and lateral) were allowed to relax as the sample was held under constant axial displacement. Tests were also run by applying a lateral load to a sample in a step fashion through turning of the frame turnbuckle assembly and observing the corresponding axial load. Again, after each load step the loads (both axial and lateral) were allowed to relax as the sample was held under the current conditions. It was found that coupling still existed between the axial and lateral load, which was thought to be due to deflection of the frame push rods. Subsequently, work was done to stiffen the frame by providing supports to the push rods.

After stiffening the test frame, tests were run by axially loading samples to a set level, then performing a lateral step loading until the sample began to slip. A summary of the failure behavior of Min-K under this testing is shown in Table 9. In general, samples began to slip when the applied lateral load was roughly twice the applied axial load. This is as expected since a friction factor of ≈ 1.0 was expected for this material and the applied lateral load was split over two sample surfaces. Therefore, the lateral load at slippage should be roughly twice the applied axial load.

Table 9. Summary of General Lateral Load Test Results After Second Modification

Sample Size (inches)	Temperature	Axial Load (lbs.)	Failure Lateral Load (lbs.)
1.0 x 1.0	RT	65	No failure up to 70 lbs.
1.0 x 1.0	ET	65	No failure up to 70 lbs.
1.0 x 1.0	RT	65/25	50
1.0 x 1.0	ET	65/25	50
1.0 x 1.0	RT	65/15	40
1.0 x 1.0	ET	65/15	30
1.0 x 1.0	ET	65/10	30
1.0 x 1.0	ET	65/25/15	30
1.0 x 1.0	RT	25	50
1.0 x 1.0	RT	25/15	40
1.0 x 1.0	RT	35/15	30
2.5 x 2.5	RT	270	No failure up to 270 lbs.
2.5 x 2.5	RT	152	No failure up to 300 lbs.
2.5 x 2.5	RT	152/95	181

RT = room temperature, ET = 400°C

3.2.4 Testing and Results Of Isothermal Stress Relaxation Testing

3.2.4.1 Experimental Procedures

Additional isothermal stress relaxation testing was performed using 6" (15 cm) diameter, 2" (5 cm) long cylindrical samples at various temperatures and loads as indicated in Table 10. Sample loading was performed in strain control utilizing a twelve-step loading scheme with loading every half hour at a rate of 5.56% strain/hour as requested by the program sponsor to simulate actual system parameters. The purpose of this testing was to provide additional information on the isothermal stress relaxation behavior of Min-K at intermediate temperatures in the range of 400-700°C. As found through previous testing¹, the behavior of Min-K transitions from "lower temperature behavior" to "higher temperature behavior" at these temperatures.

Table 10. Isothermal Stress Relaxation Test Matrix

(All samples loaded to 200 psi – 1380 kPa)

Test #	Temperature (°C)	Initial Load (lbf./N)	Test Duration (hours)
3_1	450	5,495/24,443	1,033
3_2	450	5,062/22,517	918
3_3	500	5,207/23,162	1,320
3_4	Not completed	NA	NA
3_5	450	5,479/24,372	570
3_6	500	5,695/25,333	1,006
3_7	550	5,663/25,190	456
3_8	550	5,664/25,195	749
3_9	650	5,664/25,195	724
3_10	600	5,658/25,168	24
3_11	650	5,658/25,168	1,487
3_12	600	5,728/25,479	4,676

3.2.4.2 Results

Experimental testing of Min-K under isothermal stress relaxation conditions was completed at 450, 500, 550, 600, and 650°C with an initial stress of ≈ 200 psi (1,380 kPa). The duration of these tests spanned from 24 hours to in excess of 4,675 hours. Typical results from isothermal stress relaxation testing are shown in Figure 34.

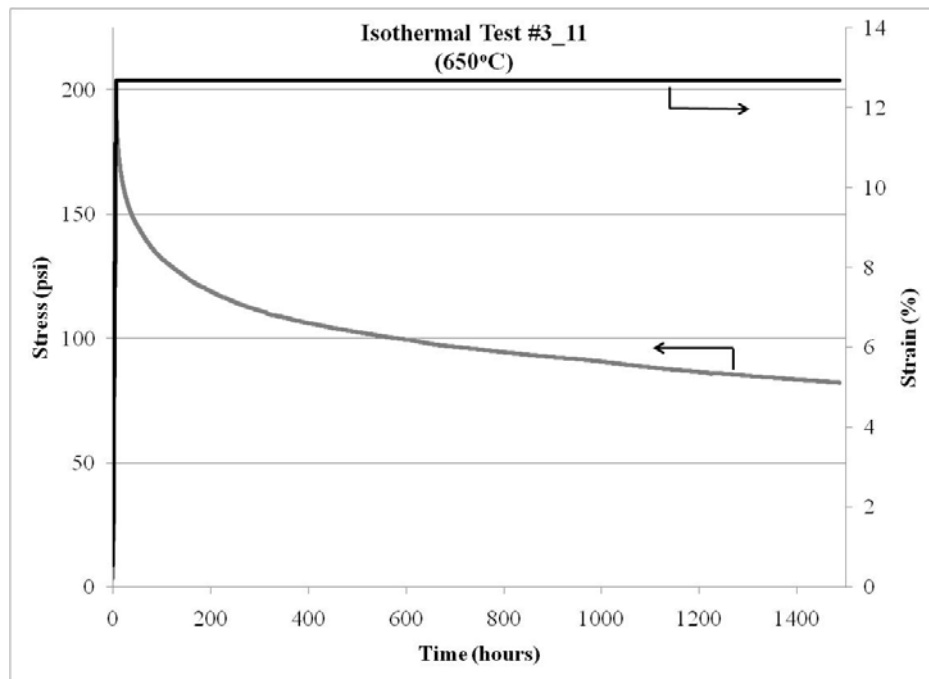


Figure 34. Isothermal Test #3_11 (650°C).

References

1. J.G. Hemrick, E. Lara-Curzio, and J.F. King, “Characterization of Min-K TE-1400 Thermal Insulation”, ORNL Technical Report, ORNL/TM-2008/089, (2008).
2. J.G. Hemrick, E. Lara-Curzio, and J.F. King, “Characterization of Min-K TE-1400 Thermal Insulation (Two-Year Gradient Stress Relaxation Testing Update)”, ORNL Technical Report, ORNL/TM-2008/157, (2009).

INTERNAL DISTRIBUTION

- | | | | |
|------|----------------|-----|------------------------------|
| 1. | E. P. George | 9. | B. R. Friske |
| 2. | J. G. Hemrick | 10. | G. R. Romanoski |
| 3. | J. M. Holladay | 11. | G. B. Ulrich |
| 4-6. | J. F. King | 12. | K. R. Veach, Jr. |
| 7. | R. G. Miller | 13. | ORNL Laboratory Records—OSTI |
| 8. | E. K. Ohriener | | |

EXTERNAL DISTRIBUTION

- 14-19. U. S. DEPARTMENT OF ENERGY, NE-43/Germantown Building, 1000 Independence Avenue S. W., Washington, District of Columbia 20585-1290
- W. A. Bohne
A. K. Caponiti
D. A. Cairns-Gallimore
W. P. Carroll
L. L. Rutger
W. S. Yoon
20. DEPARTMENT OF ENERGY, Oak Ridge Office, Building 4500N, Oak Ridge, TN 37831
- S. R. Martin, Jr., Mail Stop 6269
- 21-22. IDAHO NATIONAL LABORATORY, P. O. Box 1625, Idaho Falls, ID 83415
- S. G. Johnson
K. L. Lively
23. LOS ALAMOS NATIONAL LABORATORY, P. O. Box 1663, NMT-9, MS E502, Los Alamos, NM 87545
- D. Armstrong
- 24-25. ORBITAL SCIENCES CORPORATION, INC., 20030 Century Blvd., Suite 102, Germantown, MD 20874
- R. T. Carpenter
E. A. Skrabek
26. URS Washington Division, P. O. Box 5388, Aiken, SC 29804-5388
- J. Barber